University of Illinois at Urbana-Champaign

ACRC

Air Conditioning and Refrigeration Center   A National Science Foundation/University Cooperative Research Center

Fundamental Investigation on the Tribological Failure Mechanisms of Compressor Surfaces, Scuffing: Detailed Roughness Analysis of Al390-T6

A. Y. Suh, A. A. Polycarpou, and T. F. Conry

ACRC TR-211   March 2003

For additional information:

Air Conditioning and Refrigeration Center
University of Illinois
Mechanical & Industrial Engineering Dept.
1206 West Green Street
Urbana, IL 61801

(217) 333-3115

Abstract

Scuffing that occurs at tribological contacts in mechanical components, brings about topographical, chemical, and mechanical changes mainly at the sub-micron surface. In this project, extensive studies involving the use of various engineering and scientific tools were performed to better understand the exact mechanisms behind this phenomenon. A High Pressure Tribometer (HPT) was used to simulate shoe-on-disk tribological contacts under various conditions as encountered in compressor surfaces. Specifically, Al390-T6 disk/52100 steel pin tribo-pairs are representative of typical contacting surfaces used in swash plate-type air-conditioning compressors. Once the time to scuff a sample under the test protocol was determined, subsequent HPT tests were stopped at 0.25 x Scuffing Time, 0.50 x Scuffing Time, and 0.75 x Scuffing Time intervals. The progressive change in disk topography leading up to scuffing was first observed in the 1-D roughness study [1], but more extensively captured by the 2-D Birmingham-14 roughness characterization that is also described in this report [2]. When the chemical analyses were conducted on the uppermost surfaces for depths of 120 nm, significant changes in some of the major chemical element concentration were revealed at scuffing. The major chemical compositional changes include a depletion of silicon, which was used to strengthen the aluminum alloy, and a drastic increase of oxygen component, signaling heavy oxidation at scuffing [1]. The mechanical properties of the disks undergoing tribological evolution were also investigated through various experimental hardness measurements, ranging from macro- to micro-, and to nano-scales [3]. Based on the experimental hardness results, it was found that the hardness of the material becomes higher at the micro- and sub-micro scales than the bulk, regardless of the amount of wear towards scuffing. It was also observed that there was a gradual weakening of the uppermost 60 nm. In this report, we describe in detail the surface roughness changes that occur to the Al390-T6 samples as they undergo progressively longer tribological testing, eventually leading to scuffing.

[1]   Patel, J.J., Polycarpou, A.A., and Conry, T.F., 2002, "Investigation of the Scuffing Mechanism Under Starved Lubrication Conditions Using Macro, Meso, Micro, and Nano Analytical Techniques," ACRC TR-191, University of Illinois.

[2]   Suh, A.Y., Polycarpou, A.A., Conry, T.F., 2003, "Detailed Surface Roughness Characterization of Engineering Surfaces Undergoing Tribological Testing Leading to Scuffing," Wear, in press.

[3]   Pergande, S.R., Polycarpou, A.A., and Conry, T.F., 2002, "Use of Nano-Indentation and Nano-Scratch Techniques to Investigation Near Surface Material Properties Associated with Scuffing of Engineering Surface," ACRC TR-193, University of Illinois.

Table of Contents

List of Figures

List of Tables

Page

Chapter 1

1.1 Motivation

Real engineering surfaces are expected to withstand a wide range of temperature, various lubrication types (sometimes no lubrication), and severe contact pressure conditions. During such highly-stressed operations, prolonged surface contact may lead to abrupt catastrophic failure termed scuffing in some applications. Types of wear processes known to have a role leading to scuffing include adhesive wear, abrasive wear, fatigue wear, and corrosive wear (Patel, 2001). Scuffing, when defined during operation, is signaled by a drop in contact resistance in a critically worn state, which many times is a main source of the unexpected failure in motion (Pergande, 2001). Once the scuffing process has been initiated, friction increases drastically in the sliding contact region, which leads to catastrophic failure. In order to prevent such failure, not only is one required to observe and investigate the physical changes that happen in the material during wear and damage, but also gain insights in how damage mechanisms progress in relation to given environments, in hopes to minimize and eliminate scuffing. Factors influencing scuffing include pressure, velocity, temperature, lubrication, surface topography, materials and metallurgical aspects, and film coatings of surfaces in contact (Pergande, 2001). In recent studies, it has been proposed and shown that the most crucial damage occurs at the uppermost surface layer of engineering surfaces (50-100 nm range) (Pergande, 2001). Understanding the characteristics of the uppermost surface layer, however, is in no way a trivial pursuit, and it requires using combinations of several comprehensive techniques, i.e. topographical, chemical, micro-structural, and mechanical analysis.

One solution to preventing scuffing is to establish step-by-step design criteria, based on the results of series of experimental and analytical studies performed. The most fundamental step towards understanding the mechanisms leading to scuffing is the characterization of surface topography. Surface topography is a geometrical property of the surface. The surface finish or texturing chosen during the surface manufacturing process, and the types of wear conditions that a surface has withstood over time, are all visually indicated in the topography of the surface. Although surface roughness is usually mentioned in engineering tribological applications, the extent of its importance is perhaps underrated. Furthermore, commonly used roughness parameters in many topographic analysis are not comprehensive, generally limited to 1-D amplitude properties, e.g. Center-Line Average (CLA) and Root-Mean-Square (RMS). Since wear usually abrades the top surface and the contained features, showing a mere decreasing trend in the CLA and RMS does not surpass the intuitive expectation; it does not provide any new and significant insights into how wear damage induces topographic change contributing to catastrophic failure. Nor does this provide any justification to the decreasing trend in hardness as a compressor surface undergoes progressive wear, as shown in nanoindentation experimental results (Pergande, 2001). One solution to approaching the dilemma is to perform the more comprehensive version of 2-D surface topography characterization known as the "Birmingham-14 parameters". The Birmingham-14 parameters can be used primarily as a tool for measuring the qualitative changes in surface geometry as the surface steps through wear. One may eventually hope to use the Birmingham-14 as a tool for predicting other assumed changes that occur in internal sub-layer as well, features like hardness, elastic/plastic deformation, chemical composition, micro-structure (Stout *et al.*, 1993).

1.2 Overall Project Objectives (ACRC 127)

It has been shown in recent studies of scuffed surfaces that the most critical change in material, chemical, structural, and geometrical properties occur in the top 50 – 100 nm below the surface (Patel, 2001; Pergande, 2001). To perform the fundamental investigation of the tribological failure mechanisms, Al390-T6 disks and 52100 steel pins were used as the exemplary contacting surfaces that eventually succumbed to scuffing. The engineering materials such as the Al390-T6 and 52100 steel are representative of the contact surfaces usually found in air conditioning swash-plate compressors. The main objective of this chapter is to examine and quantify changes in topography occurring at the topmost level during wear and damage that ultimately lead to scuffing. Most recently, other experimental and analytical efforts have been performed as an extension of the analysis of the scuffing mechanism work initiated by Patel (2001). For instance, micro-structural and chemical understanding of wear and damage mechanism has been substantiated in recent nanoindentation and nanoscratch experiments on the Al390-T6 disks and 52100 steel pins, from which hardness H and elastic modulus E values are extracted empirically within the topmost layer (Pergande, 2001). Also as an ongoing project, the Finite-Element-Method has been adopted to model nanoindentation to extract other imbedded material properties such as the yield strength Y_0, as well as to develop pin-on-disk models to solve analytically the coupled thermal-mechanical problem during scuffing.

In this chapter, the topographic evolution during wear leading to scuffing is described through the characterization of amplitude, spatial, and hybrid properties of the disk surfaces. More importantly, the evolution of functional properties, i.e. bearing, sealing, lubrication retention capabilities at each tribological stage that lead to scuffing, is studied in reference to how the changes in surface topography influence its intended functional performance potentials (Stout *et al.*, 1993). The overall goal in this work is to show that the pre-established 2-D surface roughness parameters are indeed the quantitative tools for characterizing the geometric properties of a surface at various stages prior to scuffing. As it turns out, the prominent characteristics in the worn topography of the disk surfaces result in distinctive 2-D roughness parameters upon analysis.

1.3 Materials and Test Conditions

The materials used to simulate the real compressor surfaces are Al390-T6 disks and 52100 steel pins; the Al390-T6 disk, a cast aluminum with high silicon content (16.0 – 18.0 % in specified weight), is in sliding contact with the steel pin under a starved lubricated condition (Pergande, 2001). The HPT, or High Pressure Tribometer apparatus is used to simulate the real sliding/wear contact environmental conditions encountered in air conditioning compressor. The HPT is generally used to simulate run-in wear and sliding friction encountered in real engineering applications. A lower sample (pin) is stationary and in contact with an upper rotating sample (disk) in the test chamber, with the built-in ability to measure the forces in the three orthogonal directions, i.e. friction force and normal load. The HPT has the ability to vary the load up to 1000 lbf, contact temperature from -30 °C to 150 °C, as well as move between lubricated and un-lubricated tests. For more on the instrumentation specifications, see Patel's thesis (2001).

The Al390-T6 aluminum samples to be used in the 2-D roughness analysis had already been wear-tested from the previous investigation of scuffing mechanism (Patel, 2001). The basic mechanism leading to scuffing is to generate sustained contact between the steel pins and disks. Because the hardness of the steel pin is much higher

than that of the disk (Disk Bulk H = 2.5 GPa, Top 50 nm layer: H = 5 GPa), wear due to sliding contact at the interface is most visible on the disk itself (Pergande, 2001). The Al390-T6 disk is approximately 75 mm in diameter with the scuffing wear track width varying up to about 8 mm, while the 52100 steel pin is 13.5 mm in diameter. Both the 1-D and 2-D surface topography analysis are to be performed over a selected area including the wear tracks. The scuffing experiments were performed using the step-loading test procedure, i.e. 20 lb normal step-load increased with a step duration of 15 seconds at 30 mm/min sliding velocity, under starved lubrication. After executing a number of experiments to obtain the "repeatable scuffing results", the time taken to fully scuff the sample was noted and quantified as T_{scuff}. The actual experimentation time leading to scuffing was 6 minutes and 15 seconds (Patel, 2001). Keeping the same test protocols conditions and parameters, three other tests were performed in which the scuffing tests were halted at ¼ time, ½ time, and ¾ time of the total scuffing time T_{scuff}. Because the original virgin samples before the wear tests were not available, regions sufficiently away from the wear tracks were taken to be the virgin samples for the 2-D roughness analysis. A total of four HPT scuff-tested samples and their virgin counterparts are studied in this chapter using the 2-D Birmingham-14 characterization techniques, and are summarized as follows (Patel, 2001):

If T_{scuff} = time to full-scuff

- Sample 2 – virgin and worn part tested for a time duration of (¼ * T_{scuff})
- Sample 3 – virgin and worn part tested for a time duration of (½ * T_{scuff})
- Sample 4 – virgin and worn part tested for a time duration of (¾ * T_{scuff})
- Sample 5 – virgin and worn part tested until fully scuffed, or T_{scuff}
- Steel Shoe – virgin sample before HPT scuffing test

A total of nine 2-D roughness measurements are later performed, keeping in mind that there may exist sample-to-sample variation due to manufacturing and texturing processes.

Depicted in Figure 44 are the data output from the HPT previously acquired on Sample 5 performed at full scuffing condition (Patel, 2001). The *x*-axis '*t*' represents *minute*s elapsed from the beginning of the test.
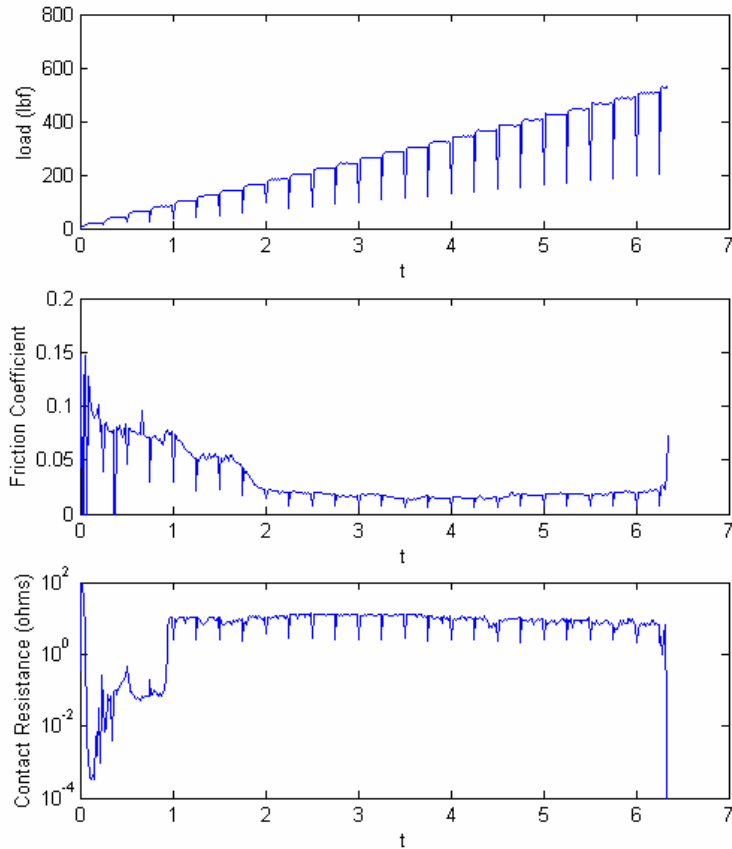
Figure 1: Typical scuffing experimental data obtained from HPT (Patel, 2001)

1.4 1-D Profile Roughness Results from Previous Studies (Patel, 2001)

In the previous investigation of wear/scuffing phenomena on the Al390-T6 disk samples, part of the emphasis was to see if any significant changes in surface topography could be noted during the wear process. By studying the disk samples that were worn at different time durations, changes were observed between the virgin state and the worn state of each sample, as well as any appreciable trends between samples worn at different time durations (Patel, 2001). The Dektak 1-D profilometer was used to obtain two orthogonal 1-D line scans of each disk, one in the direction of sliding (i.e. circumferential direction) and one in the direction across sliding (i.e. radial direction) (Patel, 2001). Each 1-D line-profiles in the circumferential direction is composed of 8000 data points, and is 1 mm in length. Subsequently, the statistical roughness parameters from four different scans on the same sample were calculated using the spectral moment method explained in Chapter 2, which were then averaged to monitor statistical variation. The plots of the Center Line Average (R_a), Root-Mean-Square (R_q), Average Radius of Curvature of Asperities (R), Areal Density of Asperities (η), Skewness, and Kurtosis from the average circumferential scan data are taken from Patel's thesis (2001), and shown in Figure 45. Note that Sample 1 is a virgin sample with no HPT scuffing test.
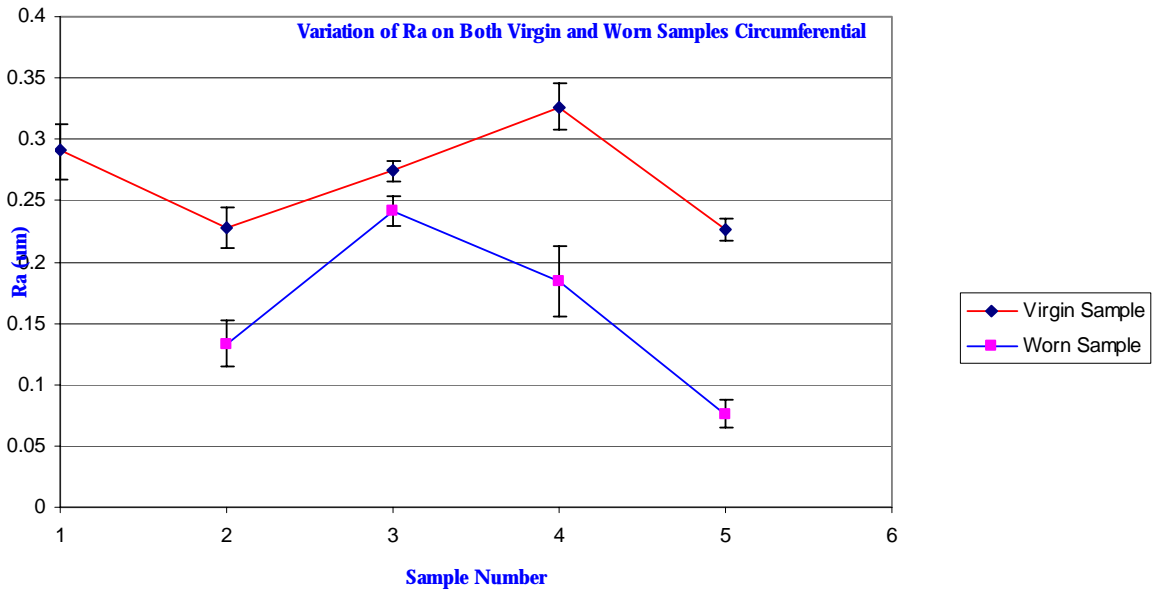
Figure 2: R_a variation on virgin/worn samples (sliding dir.) (Patel, 2001)
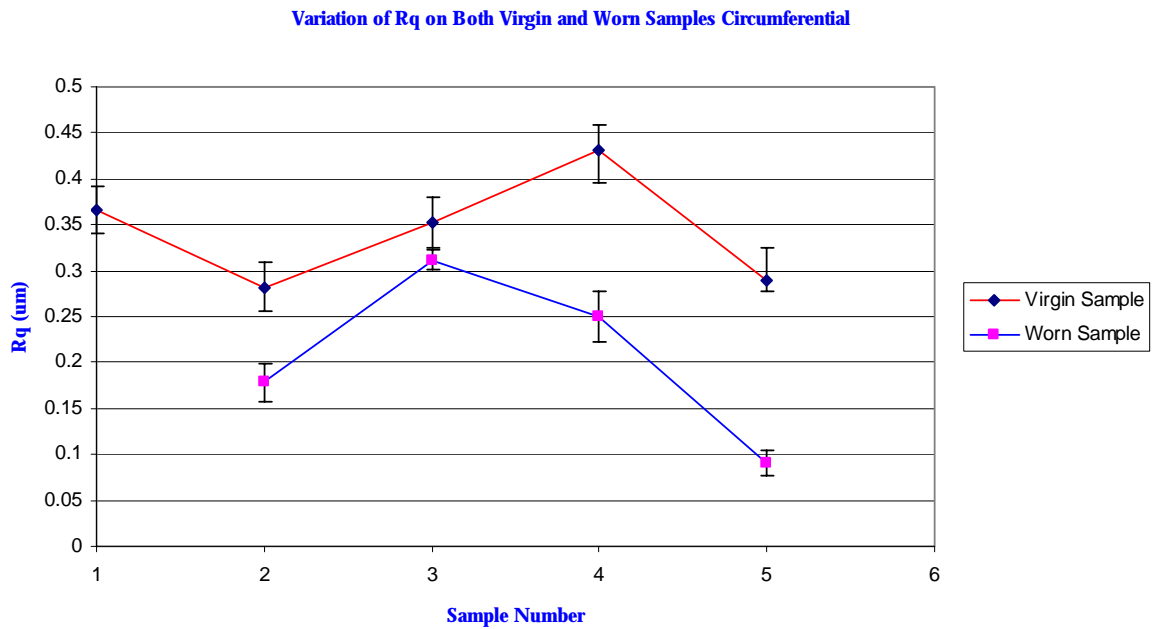
Figure 3: R_q variation on virgin/worn samples (sliding dir.) (Patel, 2001)
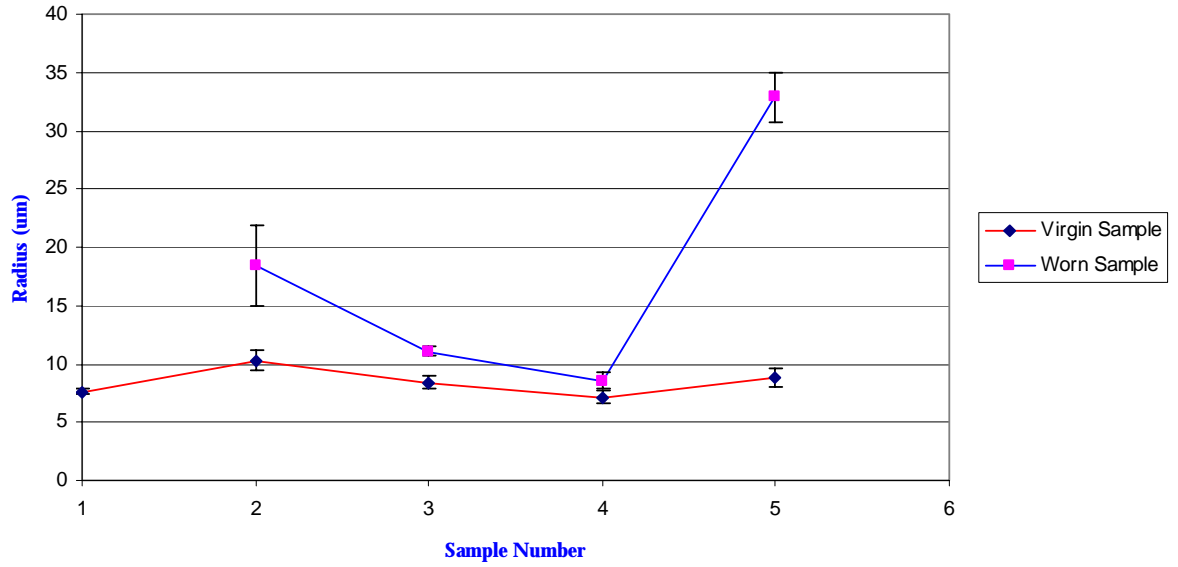
Figure 4: *R* variation on virgin/worn samples (sliding dir.) (Patel, 2001)
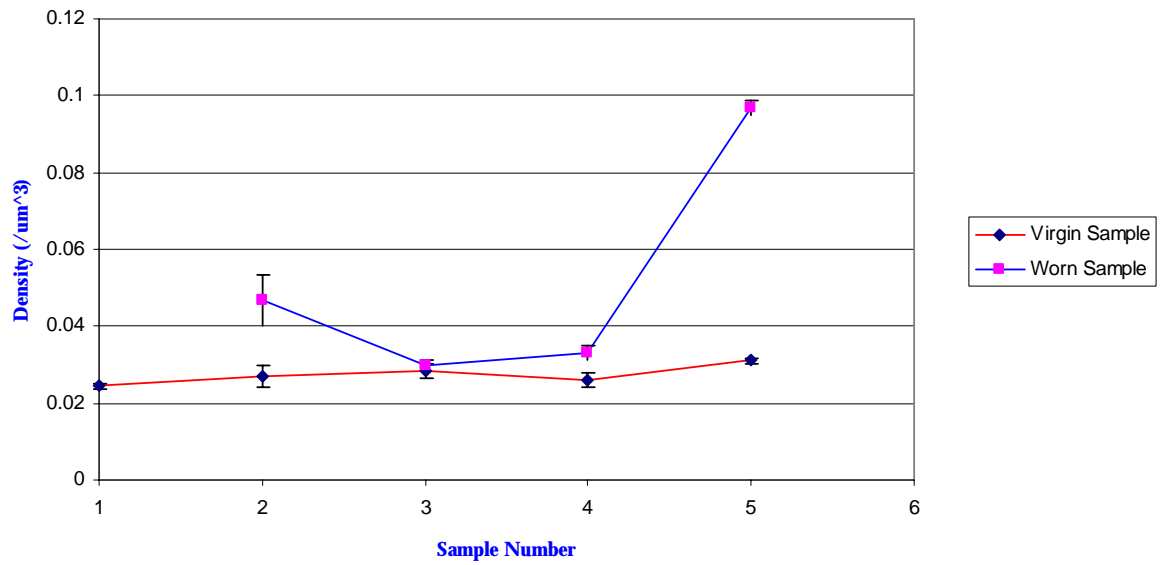
Figure 5: D_{summit} variation on virgin/worn samples (sliding dir.) (Patel, 2001)

Variation of Skewness on Both Virgin and Worn Samples Circumferential
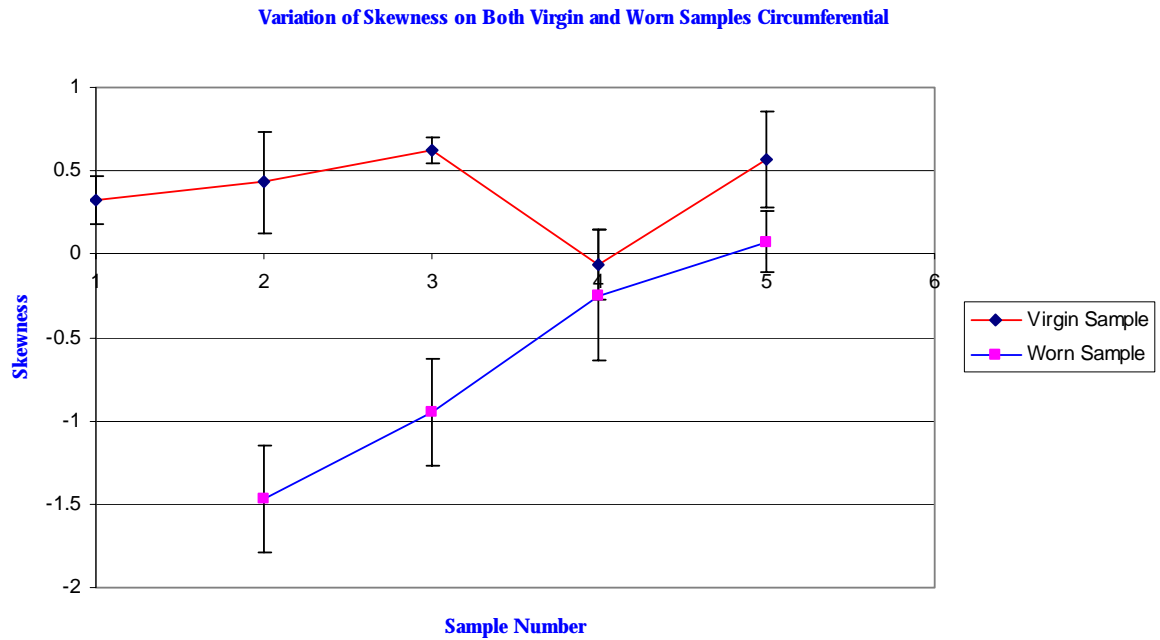
Figure 6: Skewness variation on virgin/worn samples (sliding dir.) (Patel, 2001)

Variation of Kurtosis on Both Virgin and Worn Samples Circumferential
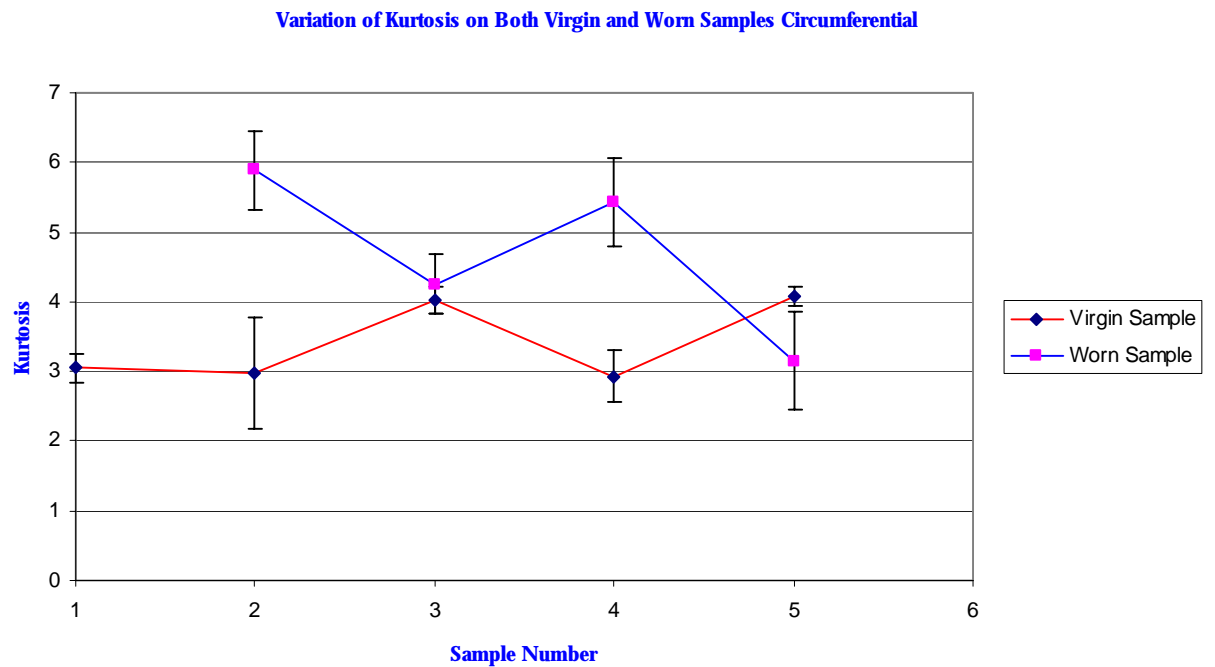
Figure 7: Kurtosis variation on virgin/worn samples (sliding dir.) (Patel, 2001)

1.5 Main Observation in 1-D Roughness Trends (Patel, 2001)

As shown in the previous 1-D roughness studies by Patel (based on the spectral methods), the wear/scuffing process brings about significant change in 1-D roughness parameters measured in the circumferential direction. For

instance, as the surface transformed from virgin to a more worn state, the R_a and R_q values seemed to generally decrease except from ¼ T_{scuff} to ½ T_{scuff} where they increased. This was attributed to the fact that the virgin ½ T_{scuff} sample (Sample 3) was rougher that the virgin ¼ T_{scuff} (Sample 2) from the start. The radius of curvature of asperities (R) and the areal density (D_{summit} or η), on the other hand, both increased almost three times - moving from ¾ T_{scuff} to T_{scuff}, or from 10 to 32 µm, and from 0.03 to 0.1 µm^{-2}, respectively. As the surface became increasingly smoother at the final stage of scuffing, the asperities were polished drastically, resulting in the increase in their radii. The sudden increase in the areal density of asperities at the final scuffing stage seemed to be, however, counterintuitive, for worn out asperities were expected to decrease the areal density. The most notable changes in 1-D roughness of the Al390-T6 disks were shown in their skewness, where for all cases the wear process caused the skewness to decrease from slightly positive values before wear to negative values after wear. As the wear progressed from worn to more worn, the skewness increased from more negative to less negative values, finally to a positive value at T_{scuff} stage. Kurtosis, however, did not yield any substantial trends.

The main conclusion from Patel's 1-D roughness study (2001) was that the surface topography is an important indication in understanding the evolution of surfaces to scuffing. This was supported by observing a few important (but not extensive) 1-D statistical parameters before and after scuffing as well as during wear leading up to scuffing. As will be seen in the remainder of this chapter, the use of the 1-D roughness parameters fails to capture the true meaning of the word "topography". The more extensive and precise investigation of the surface, the 2-D topographic analysis, is discussed in the following sections.

1.6 Importance and Motivation of the 2-D Analysis

Real life engineering contact-related problems cannot be simplified to a mere line-profile geometry due to the complexity in their contact conditions and given environments; the scuffing study of the Al390-T6 disks is no exception. Therefore, the 2-D characterization of a surface, namely, considering the surfaces as "an area with height deviation rather than a line with height deviation", becomes a necessity (Lin *et al.*, 1993). Certainly, there are other factors that may be just as important as the 2-D characterization of the surface in understanding the physical processes leading to scuffing. For instance, the air conditioning compressor surface is designed to withstand a large degree of pressure and temperature variations, sometime to a critical limit, along with varying grades of lubrication conditions, from dry to starved to lubricated. Thus, the type of material, refrigerant, and lubrication combination chosen to build the air conditioning compressor unit to achieve desired performance may be an important key to understanding the origin of scuffing. In terms of topographic analysis, the initial surface finish, whether polished or textured, may also take part in leading to different wear/scuffing related failures. For instance, depending on virgin surface finish and how the surface progressively is worn out for the duration of performance, the newly changed surface may accommodate lubricant differently; this may actually help retard or accelerate the scuffing process. Although the 1-D roughness characterization has carried us thus far, the resulting parameters lack the realistic information on spatial variation, areal and volumetric aspects of lubricant retention capabilities. This prompts one to take the next step in the roughness analysis, the 2-D roughness characterization, which can account for not only the mapping of the 2-D geometric features but also the physical and functional behavior of surface.

1.7 Roughness Image Acquisition by the Optical Profiler

Unlike micro applications, such as the head-disk interface where the surfaces are super smooth with RMS < 10 nm and the contact areas of the order of 10's of microns, most industrial engineering surfaces have roughness in the μm range and contact areas of the order of mm range. Specifically, in the case of the HPT scuffing test, the apparent contact area between the Al390-T6 disk and the steel pin is of the order of mm. Therefore, one needs a surface profiler system that can accommodate such large areas with a built-in capability to detect larger range of vertical variation due to inherently rougher topography. The most common instrument used in micro applications is the AFM; however, the AFM may not necessarily meet the much needed requirement for scanning rough surfaces. The largest scan area of the AFM, for example, is limited to only about 100 μm, which is too small for larger features and rougher amplitudes normally seen in engineering surfaces. Moreover, the vertical range of the AFM is not only limited to a couple of microns (e.g. $\pm$ 3 µm) but it cannot focus-engage onto rough surfaces. One may alternatively use a 2-D contact profilometer instead of the AFM, which has larger scanning area and vertical range. However, because the 2-D contact profilometer was not available for both the earlier 1-D (Patel, 2001) and 2-D roughness analysis, the attention was brought to using an imaging system, namely, the *optical surface profiler*.

The optical profiler is one of the most commonly used surface profilers owing to its "push-button" simplicity and quick data accumulation response. The Wyko surface profiler systems, to be specific, are non-contact optical profilers that can measure both smooth and rough surfaces with the capability to scan up to about 1.2 mm by 0.9 mm in area. One major drawback on the optical profiler is that it is based on interferometric measurements, which may not be accurate depending on the optical property of the surface different for each surface. One focus of this project is to compare directly the 2-D optical measurements with the earlier 1-D contact measurements (Patel, 2001). This ensures that the new optical measurements despite its entirely different performance criteria, are within the acceptable range, hence trustworthy.

1.7.1 Wyko NT3300 Optical Profiler System

Wyko surface profiler systems are based on interferometry techniques which make use of a white-light source. Two types of operation modes are available within the systems, i.e. phase-shifting interferometry (PSI) and vertical scanning interferometry (VSI). PSI mode is more appropriate and reliable for smooth surfaces where the height variation between two consecutive points is no more than about 160 nm (i.e. smoother surfaces). VSI mode, on the other hand, is more versatile in that it can accommodate height variation of the order of mm (i.e. rougher surfaces). For obtaining new 2-D images of the Al390-T6 disks and the 52100 steel pin, VSI mode was chosen since the peak-to-valley parameters are all in μm range. The basics of the optical imaging techniques are as follows. Light reflected from a reference mirror combines with light reflected from a sample to produce interference fringes. The system detector then measures the degree of fringe modulation (or coherence) corresponding to every focus point on the surfaces as the optical assembly and magnification moves vertically (Veeco, 1999). Table 12 summarizes system performance in VSI mode of the Wyko surface profilers (Veeco, 1999).

Table 1: System specification of the Wyko NT3300 Optical profilers

Mode	Vertical Range	Vertical Resolution
VSI	2 mm	1 – 3 nm
PSI	160 nm	1 – 3 Å

Note that compared to the angstrom vertical resolution specified in the AFM, the optical profiler systems are an order of magnitude less precise in its vertical resolution. For analyzing the Al390-T6 disks and steel shoe topography, the Wyko NT3300 Optical Profiler Series was used, and details on the sampling matrix of the obtained optical data are tabulated in Table 13.

Table 2: Sampling conditions selected in the Wyko NT3300 Optical Profiler

	x-direction	y-direction
Number of sampling points	368	240
Image Aspect Ratio	1	1.167
Image Size / Length	1.1964 mm	0.9093 mm
Sampling Interval	3.260 μm	3.804 μm

Note that the Wyko profiler systems yield more sampling points and longer image length in the *x*-direction than in the *y*-direction. The result is a rectangular image wider and richer in data in the *x*-direction. According to Stout *et al*. (1993), this condition may promote roughness results different than if the sampling conditions were the same in both directions. In order for the roughness information to have statistical significance, it was suggested the size of the data matrix should be at least 128 ($= 2^7$) in either direction when characterizing both isotropic and anisotropic surfaces (Stout *et al.*, 1993). In fact, it is recommended that in the direction of statistical significance, i.e. the direction of lay in anisotropic surfaces, the number of points can be larger than 128. As will be shown in the next section, all of the Wyko optical images taken from various scuffing stages contain texture directions due to machining marks, and this statistical significance was appropriately captured by allowing a larger number of data points to be collected in the *x*-direction ($M = 240$ vs. $N = 368$). One should also note that sampling interval values (i.e. Δx and Δy) are also different in the *x*- and *y*-directions, following an aspect ratio of 1.167 (i.e. $\Delta y = \Delta x * 1.167$). In general, given a sampling matrix, the loss of numerical and statistical accuracy that comes from the inconsistent *x* and *y* sampling intervals tends to be higher than that from the inconsistent number of data points in the *x*- and *y*-directions.

1.7.2 Wyko Optical Images

As mentioned earlier, surface topography for all of the scuffing samples with corresponding virgin parts were captured using a Wyko NT3300 Optical Profiler System. During optical scanning, no real-time digital filtering was applied to the raw images. However, a simple linear interpolation had to be applied after the imaging/data-collection to eliminate the "out of range" data values, which occur from incapacitated optical reflectivity in certain regions. Figures 51 and 52 illustrates an example for the "out of range" data (dark spots) before interpolation and the smooth "rectified" data after interpolation.
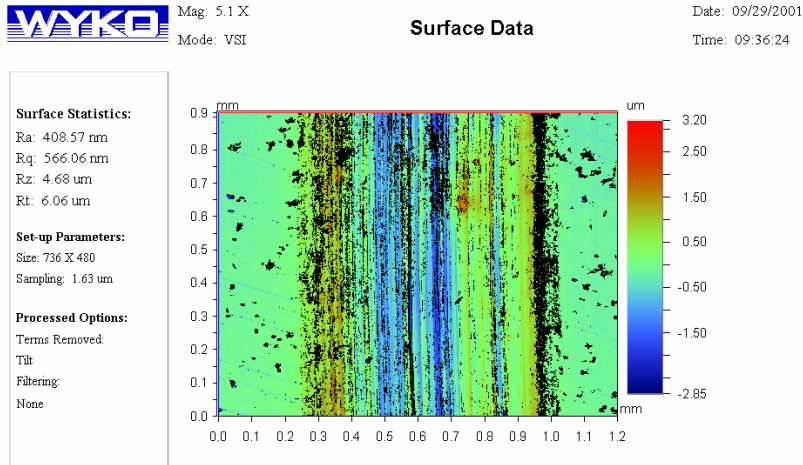
Figure 8: Typical Wyko optical image *before* linear interpolation (Fully Scuffed)
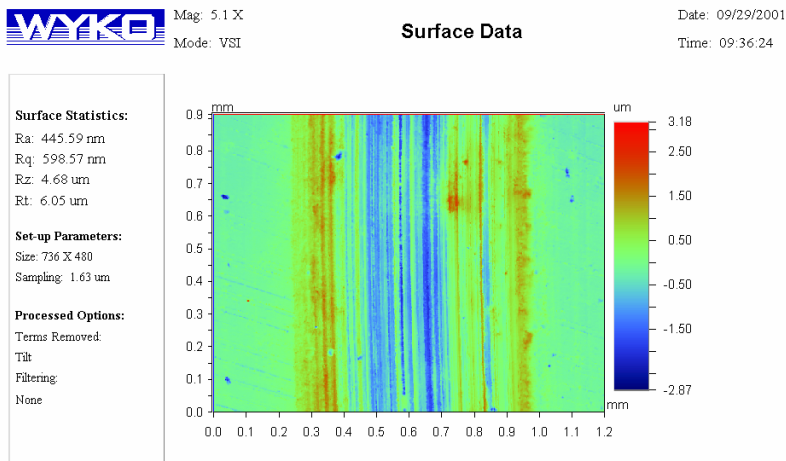
Figure 9: Typical Wyko optical image *after* linear interpolation (Fully Scuffed)

Figure 53 shows a zoomed-in image made by a high-resolution digital camera, showing the directions of sliding (red arrow) and machining on the surfaces (blue arrow) (Patel, 2001).
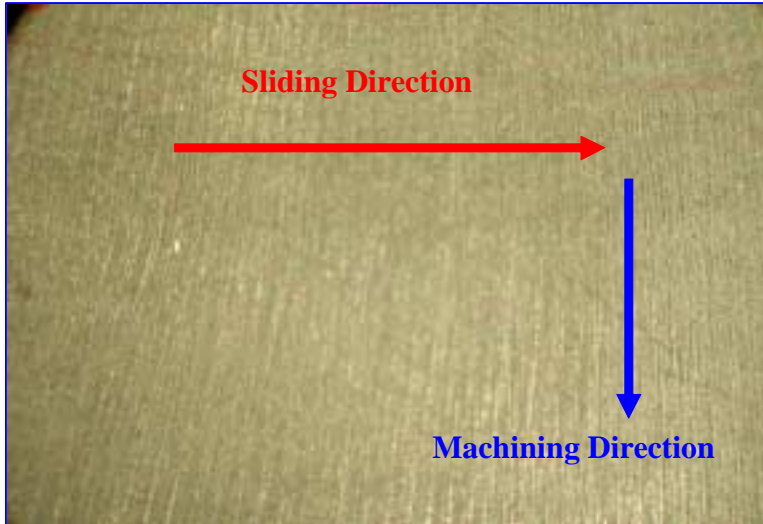
Figure 10: Sliding and machining directions on Al390-T6 disks (Patel, 2001)

Figures 54 through 61 include Samples 2 through 5 as virgin (parts not affected by the HPT scuff test) and worn (wear tracks made by the HPT scuff test) both in top and isometric views. As seen in all the images, both the virgin and worn counterparts seem to be highly anisotropic with traces of original texture from machining. Notice how the optical image of the fully-scuffed region from Sample 5 displays the wear/sliding tracks due to scuffing damage. Note that red arrows are placed on the images to denote the direction of sliding. The 2-D roughness parameters displayed inside the "Surface Statistics" box of each Wyko image stand for,

- R_a = Center Line Average, and R_q = Root Mean Square
- R_z = Average of the Ten Highest and Ten Lowest Points
- R_t = Maximum Height of the Surface
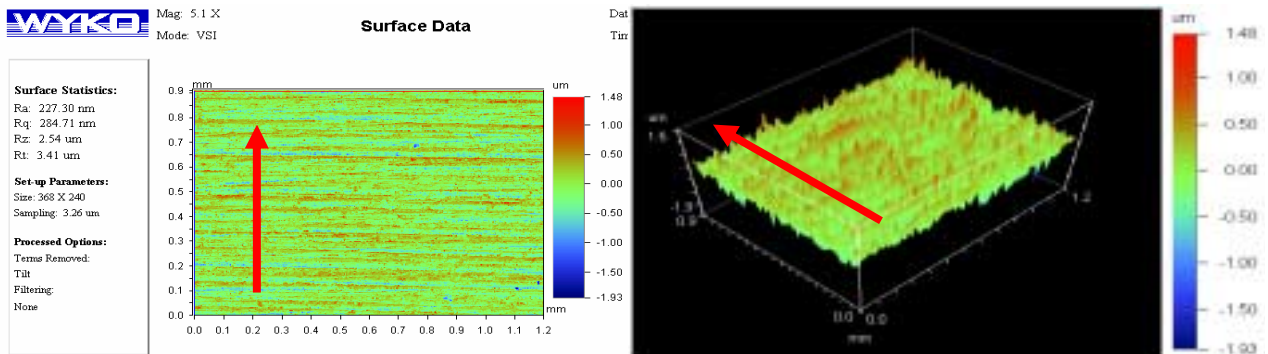
Figure 11: Wyko optical image of a virgin part of Sample 2
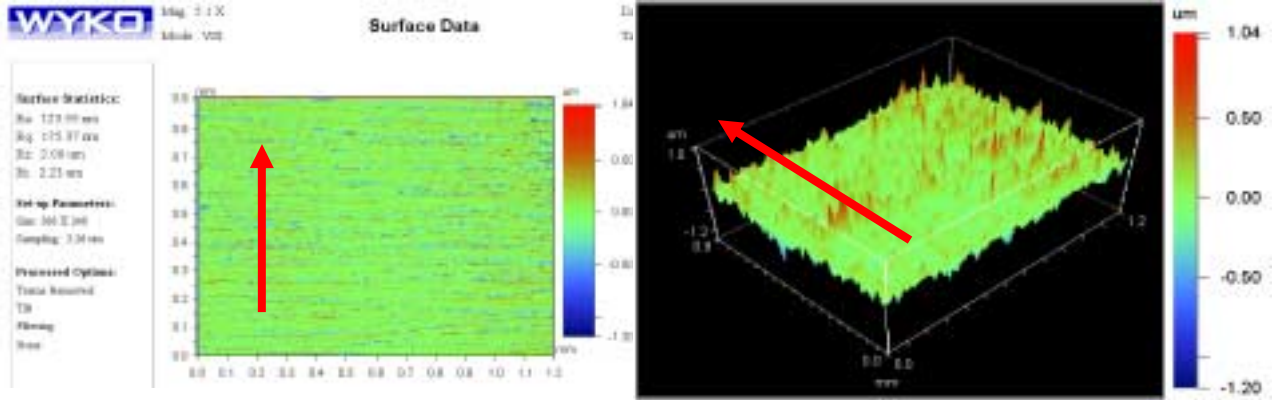
Figure 12: Wyko optical image of a worn part of Sample 2 subject to (1/4 x T_{scuff})
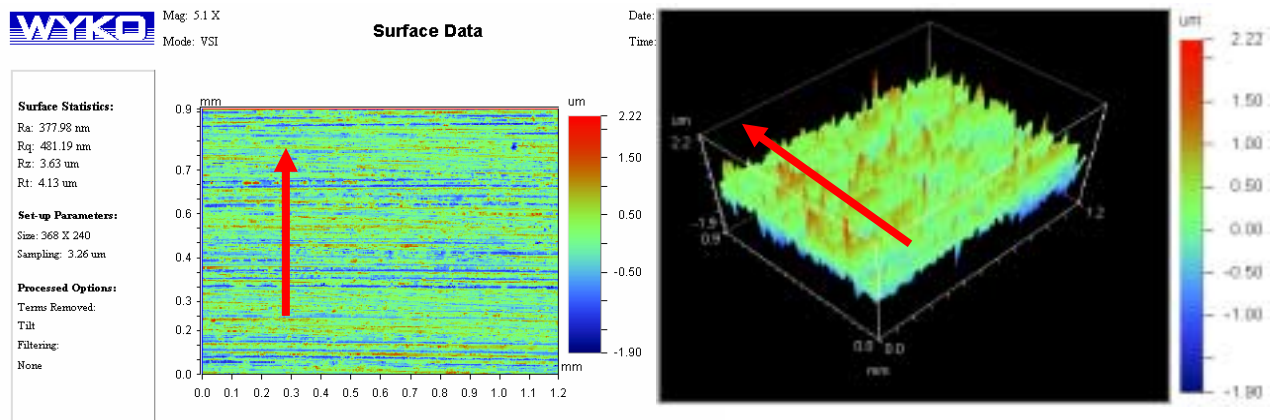
Figure 13: Wyko optical image of a virgin part of Sample 3
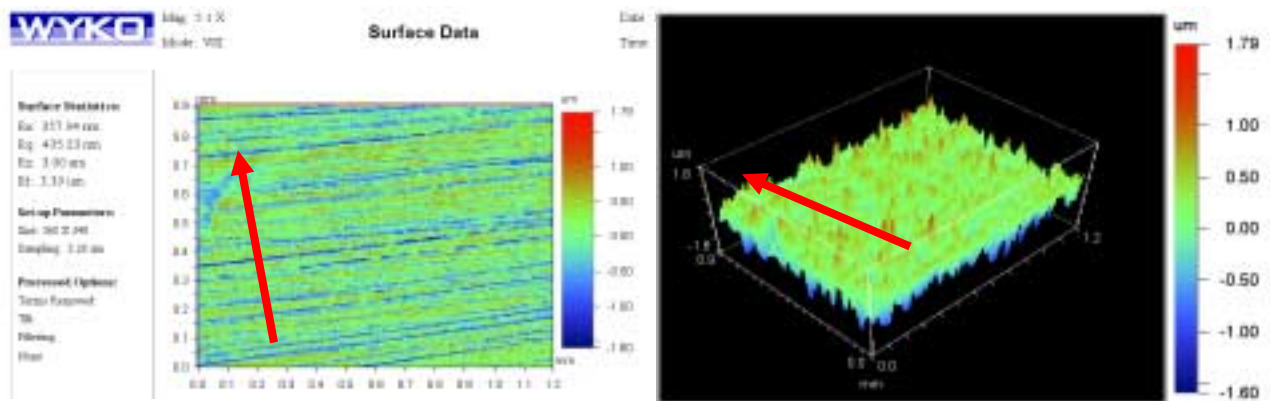
Figure 14: Wyko optical image of a worn part of Sample 3 subject to (1/2 x T_{scuff})

13
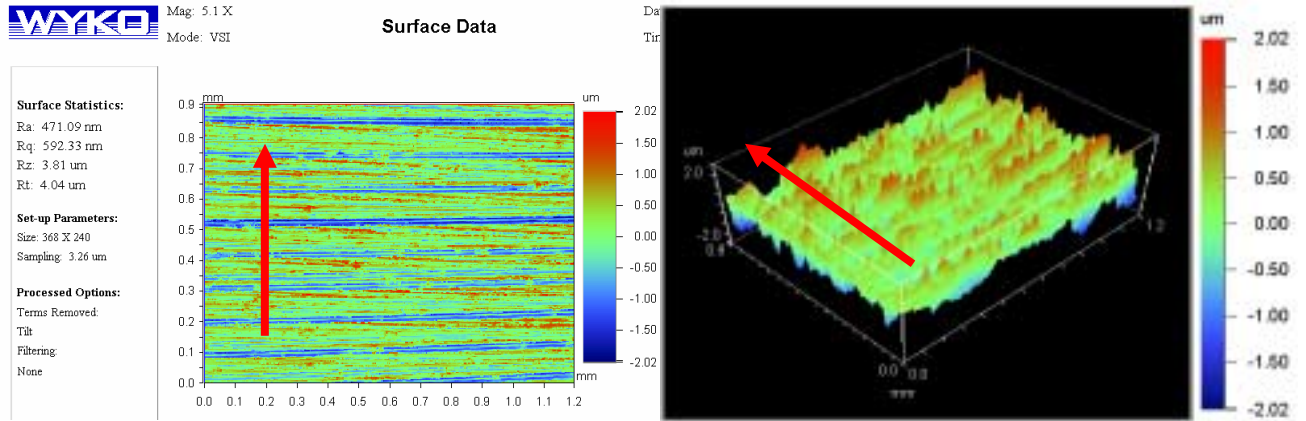
Figure 15: Wyko optical image of a virgin part of Sample 4
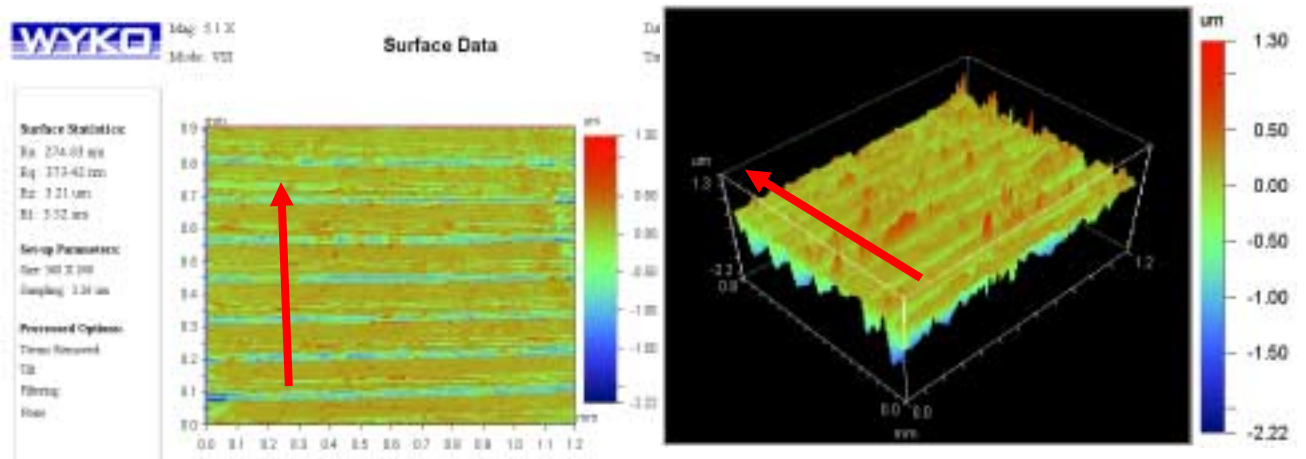
Figure 16: Wyko optical image of a worn part of Sample 4 subject to (3/4 x T_{scuff})
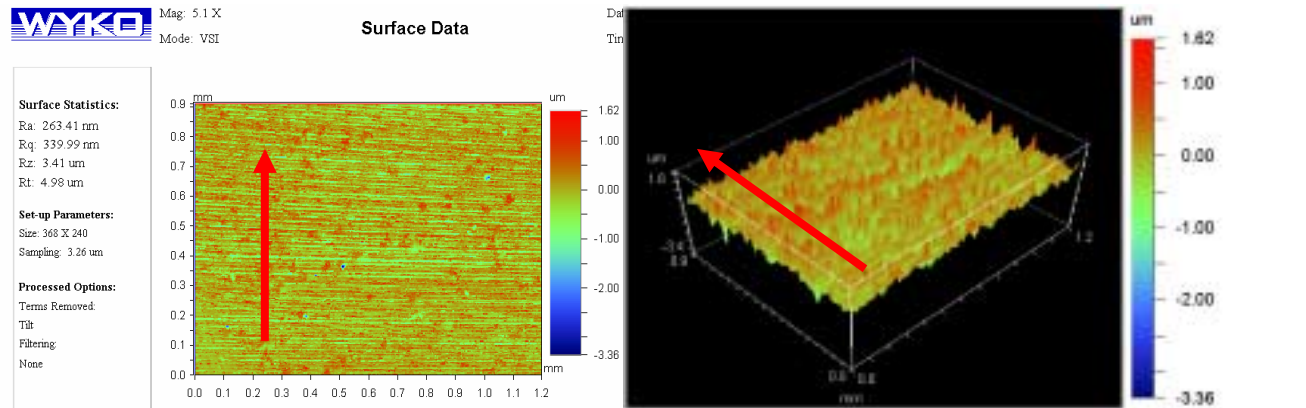
Figure 17: Wyko optical image of a virgin part of Sample 5
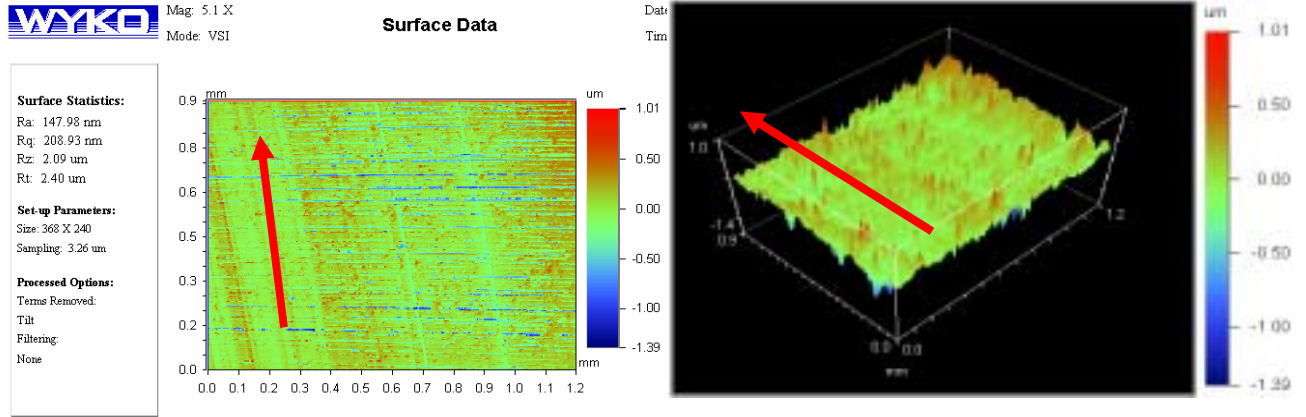
Figure 18: Wyko optical image of a worn part of Sample 5 subject to T_{scuff}
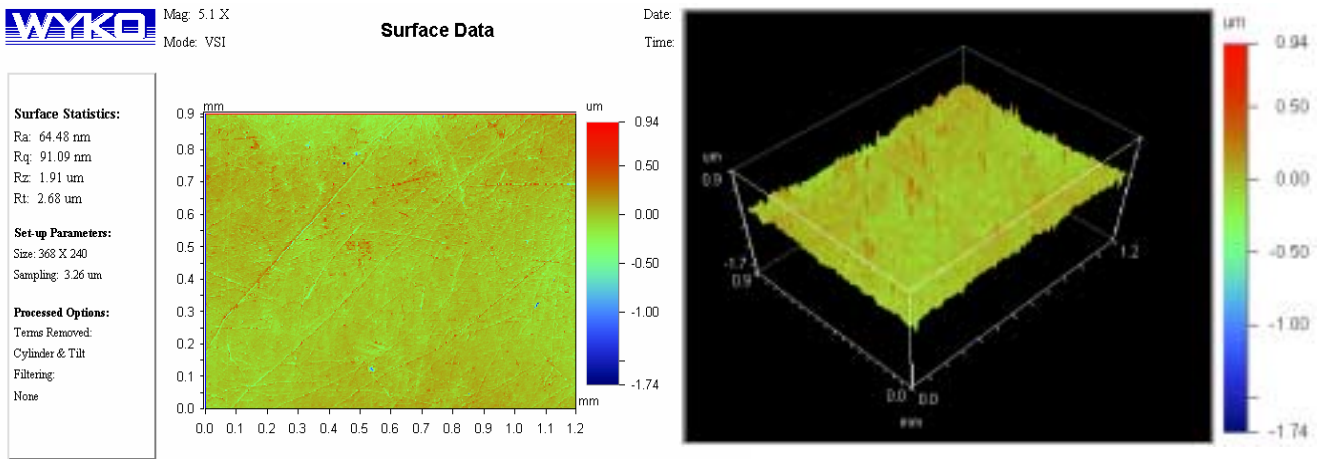
Figure 19: Wyko optical image of a virgin steel pin

All the virgin parts already have predominant directionality in their topography due to the original machining process. For all the samples, the wear/sliding direction is usually in the direction perpendicular to the machining marks. Although the machining mark on Sample 2 becomes less visible after ¼ scuffing time, the duration of wear test is not long enough to result in severe wear. One can see that the R_a and R_q values shown inside the Wyko roughness statistics boxes decrease after wear, given that the asperities in Sample 2 are simply polished.

The amplitude parameters from virgin part of Sample 3 are much higher than those from Sample 2. After undergoing ½ scuffing time, the R_a and R_q decreased only slightly and the visibility of their machining texture did not deteriorate considerably. Although there is a notable sample-to- sample variation in their virgin states, such small decrease in the R_a and R_q in Sample 3 only seems to reinforce the theory that progressive wear may accompany other topographic changes than mere change in amplitude parameters.

Upon comparing the virgin and worn images of Sample 4, the surface is smoothened out significantly after ¾ scuffing. From the isometric view of the sample, it is easily observed that the jagged top asperities are obliterated, seemingly leading to more uniformly distributed surface. Because the worn state of Sample 4 is at the point just before scuffing, the induced surface damage is expected to be much greater than just change in vertical

15

distribution of the asperities. Other topographic changes, however, cannot be realized with mere visual analysis, hence the Birmingham-14 analysis.

Upon fully scuffing, different regions on the disk exist with different topographies. When the optical capture was made to include a region of the primary wear scar on Sample 5 (Patel, 2001), an interesting observation is made. Not only did full-scuffing decrease the vertical roughness as with the other previous cases, faint scuffing tracks going in the opposite direction of the machining marks are now visible (Figure 61). Patel (2001) earlier observed and explained that at fully-scuffed state, severe wear induces material transfer between the steel shoe and aluminum in the disk sample along the "wear track," in which the surface is extremely smooth with small, defined regions. In essence, the disk sample has already failed at fully scuffed stage, thus comprehensive analysis at this stage may be irrelevant. It is more crucial, however, to observe and analyze exhaustively what happens to its surface topography *as* the disk closely approaches scuffing. Perhaps in the future, more test from ¾ T_{scuff} to T_{scuff} needs to be run to capture better the transition to scuffing.

An optical image of the virgin steel pin sample is also provided along with the disk images. Compared to the disk samples, the shoe surface possesses much smoother amplitude characteristics in terms of the shown R_a and R_q. From the top and isometric view of the pin surface provided in Figure 62, no visibly favorable texture directionality is observed.

1.8 2-D Finite-Impulse Response Low-pass Filter with Hamming Window

As a standard procedure prior to 2-D roughness analysis, all the optical topographical images are filtered using 2-D filtering techniques. After careful observation of the optical images, it is apparent that the disk surfaces exhibit no dominant "waviness" and "slope." This is perhaps due to the "non-contact" technique by which the optical profiler systems obtain images. The absence of waviness eliminates the need of High-Pass Filtering, which usually requires higher caution from the user since the cutoff wavelength designating "roughness" from "waviness" can be ambiguous and difficult at times (Stout *et al*., 1993). Therefore, only the 2-D low-pass filtering is used to filter out the high frequency noise that may be embedded in the data. The four disk samples including virgin and worn states are all equally 2-D low-pass filtered to specifically remove any wavelengths smaller than 8.5 µm. To enable fair and consistent roughness comparison, it is crucial to keep the same cutoff wavelength ranges and filtering conditions for all the optical images. On the contrary, the 2-D band-pass filtering sequence is applied to the virgin steel pin image, not only to eliminate high frequency noise (i.e. wavelength < 8.5 µm), but also to exclude the low frequency waviness originated from the gross curvature in its "flat" surface (i.e. wavelength > 20.0 µm). The filtering specifications are summarized in Table 14.

Table 3: Filtering specifications applied to the Wyko optical images

	Al390-T6 Disk Samples	52100 Steel Pin
Filter Specification	Low-Pass	Band-Pass
Filter Type	2-D FIR with Hamming Window	
Cutoff Length Range	8.5 µm and larger	8.5 µm ~ 20.0 µm

1.9 2-D Roughness Characterization Using the 2-D Birmingham Parameters

The prominent nature in the surface topography of the Al390-T6 disks at different wear stages is well-presented in both the spectral moment parameters (McCool, 1986) and the Birmingham-14 parameters (Stout *et al.*, 1993). The results are tabulated and categorized in the following sections by different roughness properties. Note that the eight nearest neighbor summit/valley definition is adopted throughout the digital calculation of summits and valleys. The notations adopted in Tables 15 to 16 simply stand for;

- **B-14** = *B*irmingham-*14*, based on the 2-D Wyko optical image (Stout *et al.*, 1993)
- **SM-EI-2D** = *S*pectral *M*oment Method developed by Sayles and Thomas, *E*quivalent *I*sotropic values based on the *2-D* Wyko optical data (averaged over each direction) (McCool, 1986)
- **SM-EI-1D =** *S*pectral *M*oment Method developed by Sayles and Thomas, *E*quivalent *I*sotropic values based on the *1-D* Dektak line scan data (McCool, 1986)

Notice that Patel's earlier 1-D roughness parameters are based on two perpendicular line scans made along and across the wear tracks, from which the 1-D equivalent isotropic parameters R_a, R_q, R, D_{summit}, Skewness, and Kurtosis are extracted using the spectral moments developed by Sayles and Thomas (1976). Patel (2001) made four different sets of 1-D perpendicular profile measurements for each disk sample (i.e. vector form) and average them for statistical credibility. In this work, the 2-D equivalent isotropic roughness parameters are also calculated along with the 2-D Birmingham-14 from the 2-D optical data, and both are compared with Patel's 1-D statistical parameters. To achieve statistical soundness and to also observe the variability within the sample, three sets of 2-D topography measurements are initially made for each sample, including virgin and worn parts. Since there appeared to be no significant variation between each measurement, only one measurement instead of all three is taken as representative of each disk sample. Although one may dispute that *one* 2-D measurement does not allow room for statistical variation, note that *one* 2-D data is already far more statistically sound and reliable than the averaged *four* 1-D data.

1.9.1 Amplitude Parameters for the Al390-T6 Disk Samples and 52100 Steel Pin

Recall that a total of nine sampling matrix (i.e. four virgin parts, four worn counterparts, and one steel pin surface) are used to calculate the corresponding 2-D surface roughness parameters, and the results are shown in Tables 15 and 16. Patel's earlier 1-D roughness parameters are also included in the table for further comparison. The details related to each parameter are thoroughly explained by McCool (1966) and also summarized in Chapter. Notice that the superscripts before some of the parameters stand for the numbering of the Birmingham-14 systems.

Table 4: Amplitude parameters of virgin Samples (2-5) and steel pin

Amplitude Parameters		Virgin Parts/Samples				
		Sample 2	Sample 3	Sample 4	Sample 5	Pin
S_a (nm)	B-14	210.75	357.29	448.03	239.13	32.62
R_a (nm)	SM-EI-2D	210.83	357.33	448.22	239.28	32.55
	SM-EI-1D	227.36	274.02	326.18	226.24	NA
[1]S_q (nm)	B-14	262.51	453.51	566.02	306.45	46.78
R_q or σ_e (nm)	SM-EI-2D	262.51	453.51	566.02	306.45	46.78
	SM-EI-1D	282.17	351.99	430.61	289.35	NA
[2]S_z (nm)	B-14	2551.96	3514.17	3667.73	3669.13	1092.09
[3]S_{sk}	B-14	-0.19	-0.16	-0.30	-0.35	-0.50
R_{sk}	SM-EI-1D	0.43	0.63	-0.061	0.57	NA
[4]S_{ku}	B-14	3.03	3.09	2.96	3.98	12.96
R_{ku}	SM-EI-1D	2.98	4.03	2.93	4.08	NA

Table 5: Amplitude parameters of worn Samples (2-5)

Amplitude Parameters		Sample 2	Sample 3	Sample 4	Sample 5
		¼ Scuffed	½ Scuffed	¾ Scuffed	Fully Scuffed
S_a (nm)	B-14	110.30	334.37	259.58	136.02
R_a (nm)	SM-EI-2D	110.33	334.40	259.52	136.03
	SM-EI-1D	133.39	242.04	184.20	76.18
[1]S_q (nm)	B-14	151.38	406.17	353.73	188.90
R_q or σ_e (nm)	SM-EI-2D	151.38	406.17	353.73	188.90
	SM-EI-1D	178.16	311.66	249.78	91.36
[2]S_z (nm)	B-14	1693.90	2811.41	3078.23	1809.85
[3]S_{sk}	B-14	-0.61	-0.43	-1.74	-1.07
R_{sk}	SM-EI-1D	-1.47	-0.95	-0.25	0.074
[4]S_{ku}	B-14	5.15	2.70	5.77	5.62
R_{ku}	SM-EI-1D	5.90	4.25	5.43	3.15

Recall that the notation for each parameter stands for,

- S_a, R_a = Arithmetic Mean Deviation of the Surface and Profile, respectively (Stout et al., 1993)
- [1]S_q, R_q = Root-Mean-Square Deviation of the Surface and Profile, respectively (Stout et al., 1993)σ_e = Equivalent Isotropic Standard Deviation of the Summit Heights based on Spectral Moment Methods (McCool, 1986)
- [2]S_z = Ten Point Heights of the Surface (Stout et al., 1993)

- **[3]S_{sk}, R_{sk}** = Skewness of Topography Height Distribution of the Surface and Profile, respectively (Stout et al., 1993)
- **[4]S_{ku}, R_{ku}** = Kurtosis of Topography Height Distribution of the Surface and Profile, respectively (Stout et al., 1993)

1.9.1.1 S_a (CLA) and [1]S_q (RMS) Trends and Analysis

The following two plots summarize the trends for the S_a (CLA) and S_q (RMS) from disk to disk and from virgin to worn stage within sample. The S_a and S_q parameters are the most fundamental and widely used amplitude parameters. As shown in Table 15 and 16, the resulting S_a vs. R_a and S_q vs. R_q (or σ_e) values from the 2-D digital methods and 2-D spectral moments, respectively, are nearly the same, though the calculation methods are entirely different. Moreover, despite the obvious dimensional discrepancy (i.e. 2-D vs. 1-D) and the number of data points used in Patel's and in this work, Patel's 1-D values (shown in Section 4.4) and the author's corresponding 2-D values have the same trends, i.e. decreasing S_a (CLA) and S_q (RMS). From both the virgin and worn S_a and S_q results, it is possible to generalize their trends as the surface is worn out progressively. For instance, in Figures 63 and 64, the S_a and S_q reduces from virgin to worn for all samples, indicating that the asperities are indeed getting polished as they are smoothened out. To better show the wear evolution starting from the virgin state leading to scuffing, Figure 63 and 64 also includes Sample 1 values, the sample with no HPT wear test performed on it. Whereas the 1-D R_a and R_q values for Sample 1 are the values extracted from actually measured line data (Patel, 2001), the 2-D S_a and S_q values for Sample 1 are the arithmetically averaged value from the other four virgin values, i.e.

$$\left(R_a\right)_{sample\ 1}^{virgin} = \left[\frac{\left(R_a\right)_{measurement\ 1}^{virgin} + \left(R_a\right)_{measurement\ 1}^{virgin} + \left(R_a\right)_{measurement\ 1}^{virgin} + \left(R_a\right)_{measurement\ 1}^{virgin}}{4}\right]_{1-D}^{circuferential}$$

$$\left(R_q\right)_{sample\ 1}^{virgin} = \left[\frac{\left(R_q\right)_{measurement\ 1}^{virgin} + \left(R_q\right)_{measurement\ 1}^{virgin} + \left(R_q\right)_{measurement\ 1}^{virgin} + \left(R_q\right)_{measurement\ 1}^{virgin}}{4}\right]_{1-D}^{circuferential}$$

$$\left(S_a\right)_{sample\ 1}^{virgin} = \left[\frac{\left(S_a\right)_{sample\ 2}^{virgin} + \left(S_a\right)_{sample\ 3}^{virgin} + \left(S_a\right)_{sample\ 4}^{virgin} + \left(S_a\right)_{sample\ 5}^{virgin}}{4}\right]_{2-D}$$

$$\left(S_q\right)_{sample\ 1}^{virgin} = \left[\frac{\left(S_q\right)_{sample\ 2}^{virgin} + \left(S_q\right)_{sample\ 3}^{virgin} + \left(S_q\right)_{sample\ 4}^{virgin} + \left(S_q\right)_{sample\ 5}^{virgin}}{4}\right]_{2-D}$$

As for going from less worn to more worn stages, a somewhat counterintuitive trend is observed. When going from ¼ to ½ scuffed, for instance, the S_a and S_q increase despite the wear of peak asperities as the surface gets polished. This can be attributed to the disk-to-disk variation in the original virgin samples. Since the S_a and S_q of the virgin Sample 3 were larger than those of Sample 2, they must increase, notwithstanding the increase in wear; it is the change within samples that is important. When surface undergoes from ½ to ¾ scuffed stages, a more reasonable trend is observed; although the S_a and S_q of the virgin ¾ scuffed were higher, those of the worn state

decreased drastically from ½ scuffed. This large reduction in both the S_a and S_q at ¾ scuffed stage seems to indicate a major wear of peak asperities just before scuffing. As for going from ¾ to fully scuffed, the S_a and S_q continue to decrease steadily, enhancing the progressive wear behavior in the top part of asperities.

From the progressive wear trends of the S_a and S_q, one can conclude *qualitatively* rather than *quantitatively*, that the surface does undergo wear, and its simple vertical topographic change is captured by these two parameters. Therefore, it would be erroneous to generalize the performance potential of these disks solely based only on the evolution of the S_a and S_q, due to the lack of information other than the vertical variation contained in the parameters. For instance, the indication of material transfer between the shoe and disk and their pile-up is in no way delineated in these basic amplitude parameters. Other than wear, which leads to smoothening of the surface, no clear trend is evident. In addition, what the S_a and S_q show is that 1-D and 2-D makes no difference in roughness analysis. Perhaps other amplitude parameters can reveal amplitude trends more quantitatively, such as the parameter S_z, which will be studied next.
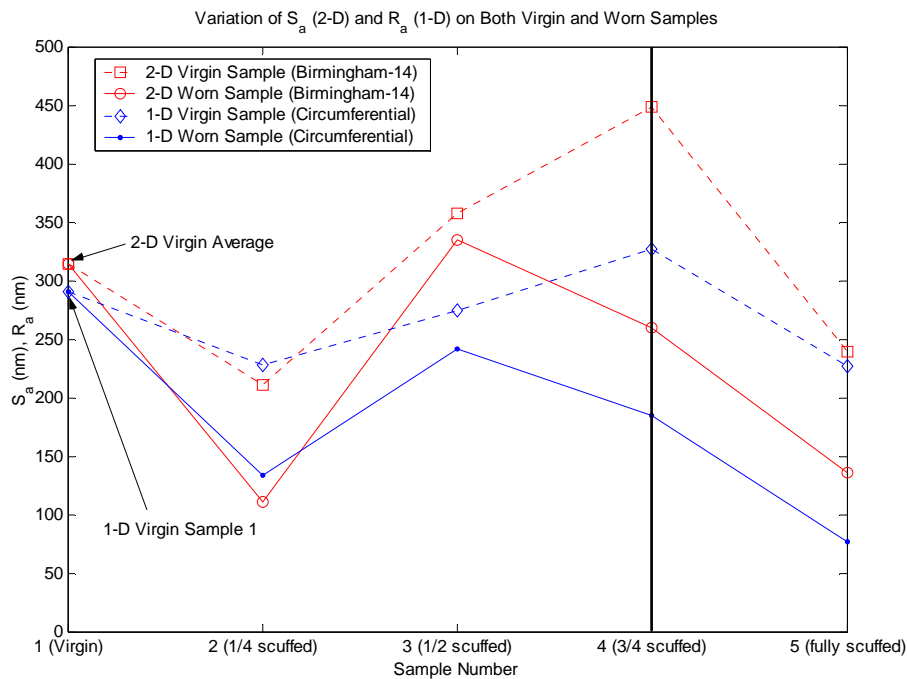
Figure 20: Variation of S_a (2-D) vs. R_a (1-D) on virgin and worn samples
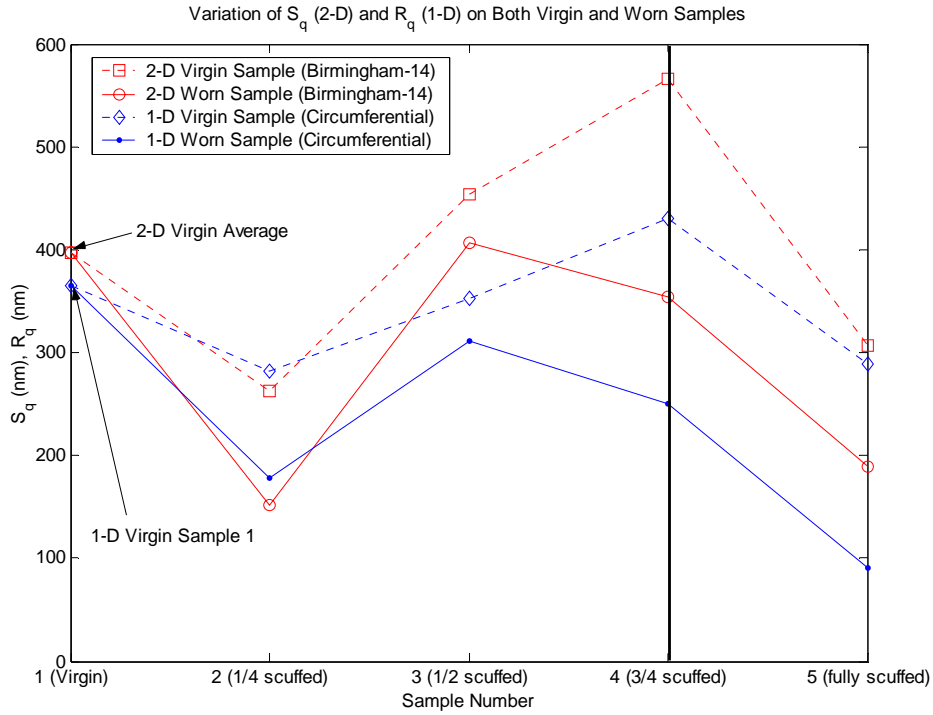
Figure 21: Variation of S_q (2-D) vs. R_q (1-D) on virgin and worn samples

1.9.1.2 ^2S_z (Ten-Point Height of the Surface) Trends and Analysis

The S_z or ten-point height variation of the surface is a parameter purely based on digital techniques. After averaging the ten most pronounced peaks and valleys using the eight-nearest summit/valley definition, the S_z trends for the disks are plotted in Figure 65. Contrary to the previous S_a and S_q analysis, the disk-to-disk variation in the virgin disks is minimized in the S_z analysis. Notice how the virgin S_z for all samples except for Sample 2 are very close to one another. As for going from virgin to worn state within a sample, the worn S_z is always smaller than the virgin S_z. Although the decrease in the worn states is also observed in the previous S_a and S_q analysis, the amount of the drop in the worn S_z in each stage is nearly identical. At fully scuffed stage, the S_z varies most drastically from its virgin state because of the major scuffing damage. However, since the fully scuffed sample is so drastically changed and has already failed at this stage, its S_z value should be disregarded from the analysis.
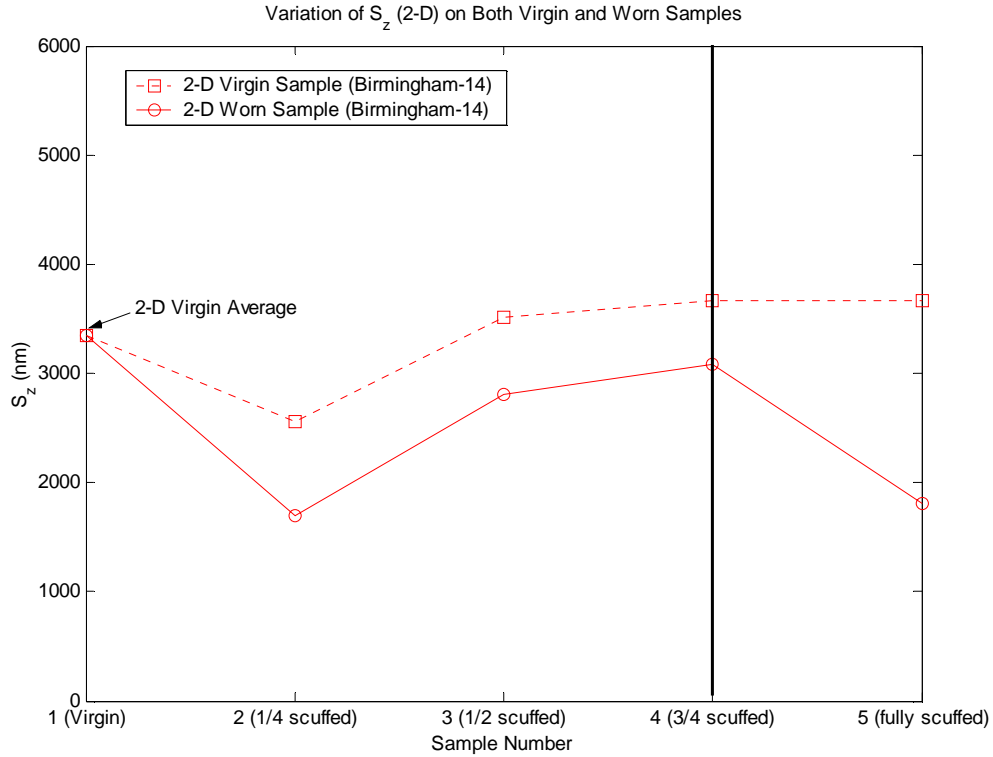
Figure 22: Variation of S_z (2-D) on virgin and worn samples

The general trend (up to ¾ scuffed) is that as the surface starts getting worn, the S_z initially decreases but it increases steadily as it is more worn. Since the S_a and S_q values are quite sensitive to disk-to-disk variation, one may consider the S_z to be a more appropriate amplitude parameter when determining the surface wear evolution, as the S_z results in more uniform wear behavior.

1.9.1.3 [3]S_{sk} (Skewness) and [4]S_{ku} (Kurtosis) Trends and Analysis

While the trends or behaviors of the S_a (CLA) and S_q (RMS) are the same for 1-D and 2-D, those of skewness and kurtosis are considerably different for 1-D and 2-D. In fact, skewness and kurtosis are the amplitude parameters that vary most between the 1-D line-profiles analysis and the 2-D areal analysis. In Patel's previously reported 1-D roughness study, all virgin disk surfaces exhibited positive skewness due to "regular" mild wear-in, with a notable sample-to-sample variation (Patel, 2001). In this work, 2-D skewness or S_{sk} values for all the virgin counterparts are negative, though they are very close to being zero (i.e. Gaussian). Moreover, sample-to-sample variation in the virgin S_{sk} appears to be insignificant in contrast to Patel's 1-D study. Information contained in two 1-D profiles in the orthogonal direction does not include all the spiky features exhibited on the surface. On the other hand, given a sufficiently large scan area, 2-D data can contain more realistic information.

Between virgin and worn states, the S_{sk} decreases for all the samples. The highly negative S_{sk} values in the worn states support the theory that polished asperities turn the surface more negatively skewed by revealing more pits than peaks. The most change is observed when moving from ½ scuffed to ¾ scuffed. At this worn stage just before full scuffing, wearing of the surface seems to be characterized by losing the spikiness of the top asperities by

22

significant amount. As for moving from ¾ scuffed to fully scuffed stages, the S_{sk} increases though not as much as moving from ¼ and ½ scuffed stages.   The reason for the mild increase at fully scuffed stage is that the hidden peaks at the lower region are now being revealed after most of top asperities are worn out and broken.   Statistically, this lowers the original mean plane, and with this change in the mean plane is the slight increase in the S_{sk} at fully scuffed stage. However, one must keep in mind that at scuffing all is possible, despite the given explanation for the increase shown in Figure 66.

The trend for the S_{ku} seems to differ a lot, when compared with the S_{sk} trend and Patel's 1-D kurtosis analysis. The S_{ku} for all the virgin states are near Gaussian (i.e. $S_{ku} \approx 3$), except in Sample 5, in which the S_{ku} is slightly centrally distributed ($S_{ku} \approx 4$). Between the individual virgin and worn states, the S_{ku} increases except in Sample 2 or at ½ scuffed. Determining a noticeable trend with the S_{ku} is especially difficult because of this sudden decrease at the ½ scuffed. This rather erratic behavior at ½ scuffed stage may be attributed to a possibly unusual sample variation in its virgin state of Sample 3, whose effect is somehow amplified in kurtosis calculation and is otherwise shown not as significant in other 2-D amplitude parameters. Or, perhaps it is simply difficult or inadequate to say anything conclusively with one measurement albeit 2-D. When going from ¾ scuffed to fully scuffed, the S_{ku} remains nearly constant as being highly centrally distributed. In general, sample variation perhaps appears to influence the S_{ku} more than it does for other amplitude properties, thereby making it difficult to draw any solid conclusion in its analysis.
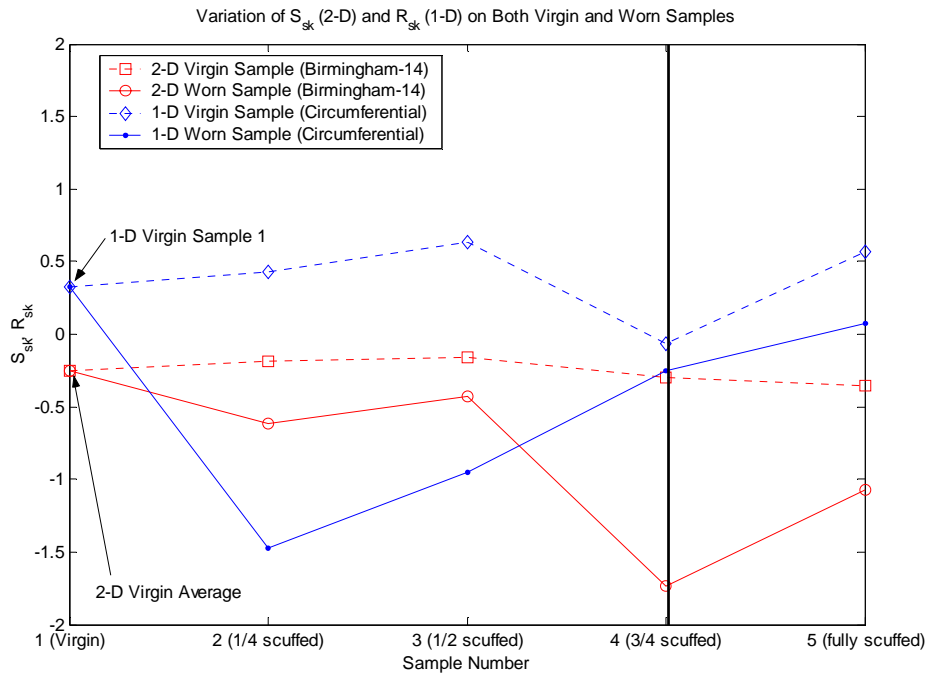
Figure 23: Variation of S_{sk} (2-D) and R_{sk} (1-D) on virgin and worn samples
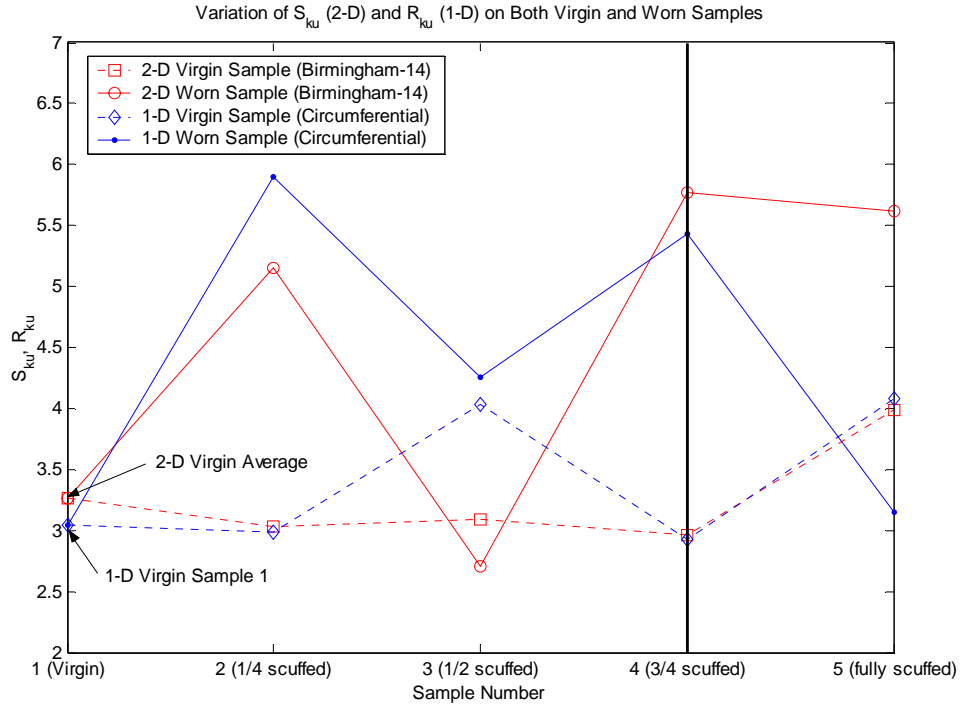
Figure 24: Variation of S_{ku} (2-D) and R_{ku} (1-D) on virgin and worn samples

1.9.2 Spatial Parameters for the Al390-T6 Samples

Spatial parameters are particularly useful in the roughness study of the Al390-T6 disks because of their uniquely defined anisotropic texture with directionality. The Areal Autocorrelation Function (AACF) and Areal Power Spectrum Density (APSD) are used to capture the well-defined anisotropy in all the disk samples (Stout *et al.*, 1993). Tables 17 and 18 summarize the 2-D spatial parameters calculated in this study as well as the 1-D spatial parameters extracted by Patel (2001), where

- [5]S_{ds} = Density of Summits of the Surface (Stout et al., 1993)
- $D_{summit, e}$ = Equivalent Isotropic Surface Summit Density (McCool, 1986)
- [6]S_{tr} = Texture Aspect Ratio (Stout et al., 1993)
- γ = Isotropic Index (McCool, 1986)
- [7]S_{td} = Texture Direction (Stout et al., 1993)
- [8]S_{al} = The Fastest Decay Autocorrelation Length (Stout et al., 1993)

Table 6: Spatial parameters of virgin Samples (2-5) and steel pin

Spatial Parameters		Virgin Parts/Samples				
		Sample 2	Sample 3	Sample 4	Sample 5	Pin
$^5S_{ds}$ (μm^{-2})	B-14	5089.15	4776.98	4690.09	5586.91	7177.81
$D_{summit,e}$ (mm^{-2})	SM-EI-2D	4129.76	3923.27	3960.67	4382.71	5118.20
	SM-EI-1D	26909.25	29767.00	25941.00	31022.50	NA
$^6S_{tr}$	B-14	0.28	0.094	0.28	0.036	0.68
γ	SM-EI-2D	0.58	0.43	0.30	0.45	0.93
$^7S_{td}$ ($°$)	B-14	-88.32	-89.16	88.32	-88.05	[1]none
$^8S_{al}$ (μm)	B-14	94.62	32.82	129.84	5.01	2.77

[1]When the $S_{tr} > 0.5$ (highly isotropic), S_{td} (texture direction) is meaningless, since there is no definite directionality.

Table 7: Spatial parameters of worn Samples (2-5)

Spatial Parameters		Sample 2	Sample 3	Sample 4	Sample 5
		¼ Scuffed	½ Scuffed	¾ Scuffed	Fully Scuffed
$^5S_{ds}$ (μm^{-2})	B-14	5656.64	4969.00	5769.28	5156.74
$D_{summit,e}$ (mm^{-2})	SM-EI-2D	4439.35	3940.42	4200.45	4163.420
	SM-EI-1D	46650.25	29767.00	32952.25	97014.50
$^6S_{tr}$	B-14	0.12	0.041	0.28	0.070
γ	SM-EI-2D	0.53	0.44	0.32	0.46
$^7S_{td}$ ($°$)	B-14	-85.01	83.15	89.37	-89.27
$^8S_{al}$ (nm)	B-14	4044.68	13.58	125.55	10493.90

1.9.2.1 $^5S_{ds}$ (Density of Summits of the Surface) Trends and Analysis

Using the eight nearest neighbor summit/valley definitions, the density of summits are calculated for all the disk samples (and the steel pin) for virgin and worn samples. As shown in Tables 17 and 18, for all the disk samples the 1-D and 2-D $D_{summit,e}$ values calculated by the spectral moments (McCool, 1986) are comparatively lower than the S_{ds} value. This is due to the differences in their methods of calculations; while the S_{ds} is calculated by explicitly allocating summits based on the chosen digital summit definition, the 1-D $D_{summit,e}$ is calculated by implicit "spectral moments" without explicitly defining summits (McCool, 1986). Nevertheless, both the S_{ds} and (2-D) $D_{summit,e}$ and values seem to produce similar trends. Despite minor variation from sample to sample in their virgin states, it is clear that the S_{ds} of the worn states are higher albeit not by much. The decrease in the worn S_{ds} at ½ scuffed is probably due to the sample variation and not an actually decreasing S_{ds} trend. At ¾ scuffed and fully scuffed stages are where most changes occur. The S_{ds} at ¾ scuffed confirms the theory that as the surface smoothens out thereby revealing more minor asperities in the lower zones, the total density of summits is increased in turn caused by the increase in the number of summits.

At fully scuffed stage, however, not only does the S_{ds} suddenly decrease in its wear trend but also below its virgin state. This is probably due to the fact that the scuffing mechanism has now successfully reached the asperities located below the mean plane, thereby reducing the number of total surviving asperities, which decreases the total density of summits, or S_{ds}. Furthermore, transfer of material and exposure of "new" material, and etc., may have influenced the total density of summits at fully scuffed stage. Figure 68 includes the plots of 2-D $D_{summit,e}$ and S_{ds}, as well as the earlier 1-D $D_{summit,e}$ trends done by Patel (2001).
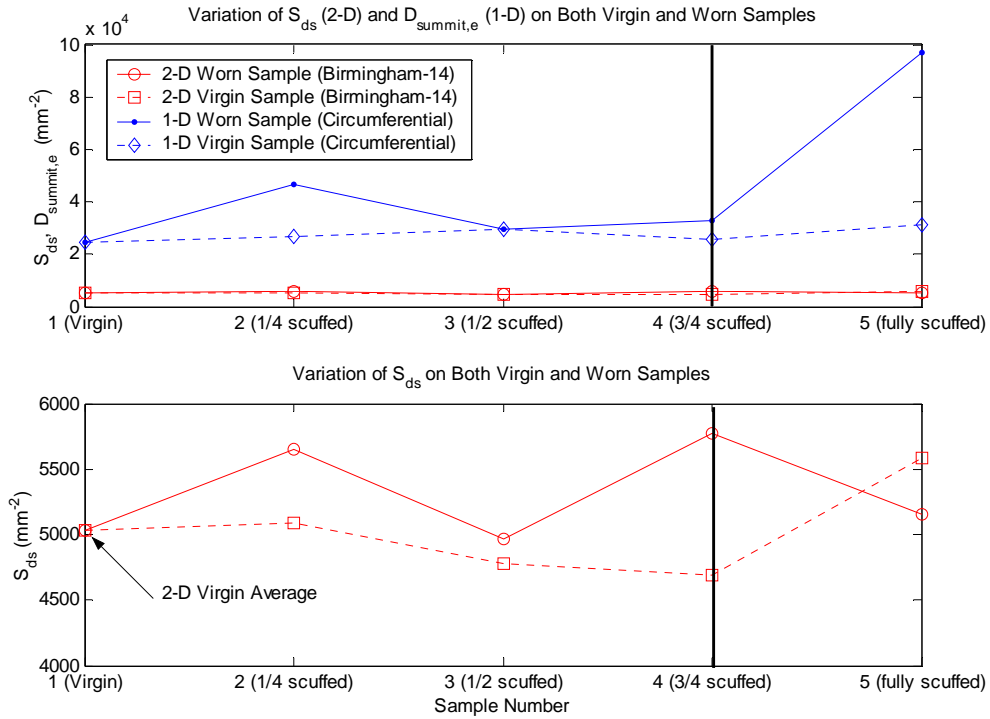
Figure 25: Variation of S_{ds} (2-D) and $D_{summit,\,e}$ (1-D) on virgin and worn samples

1.9.2.2 [6]S_{tr} (Texture Aspect Ratio) Trends and Analysis

Since the isotropic index γ values based on Patel's line scan measurements are not available, only the isotropic index γ and texture aspect ratio S_{tr} based on the 2-D optical images are compared in this work. Unlike the previous parametric comparisons in which similar values and trends are observed, the γ and S_{tr} seem to disagree most.
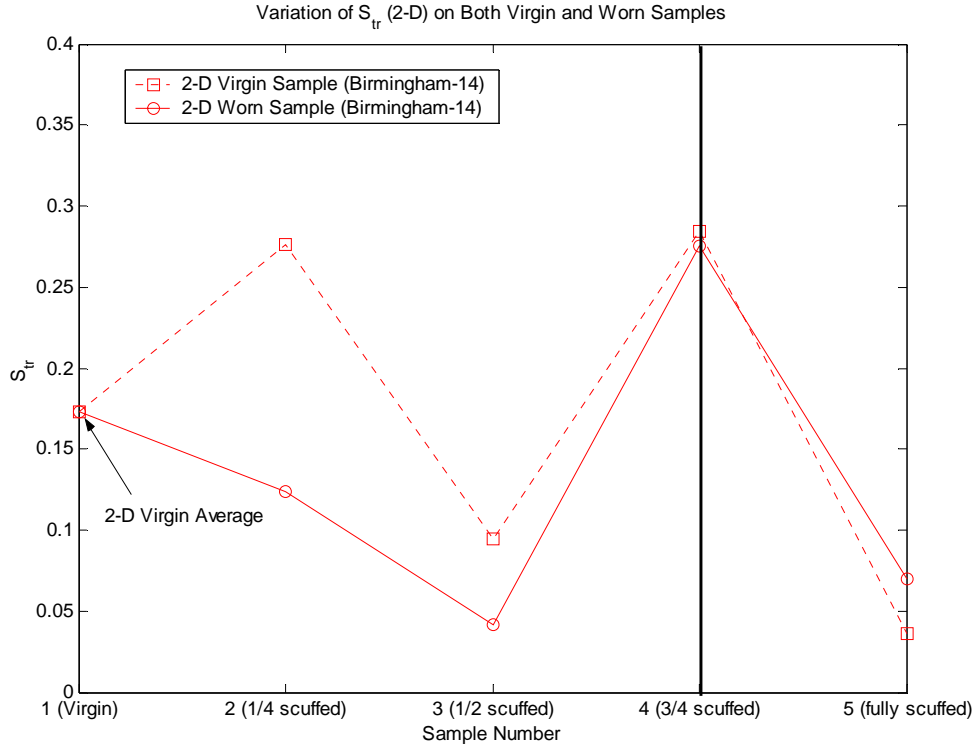
Figure 26: Variation of S_{tr} (2-D) on virgin and worn samples

It appears that the differences in the computational and theoretical approaches taken to calculate the respective the texture aspect ratio (S_{tr}) and isotropic index (γ), are most influential when determining the measure of texture isotropy. Their individual definitions are recapitulated from Chapter 2 as below:

Isotropic Index or γ

$$0 < \gamma = \left(\frac{(m_2)_{min}}{(m_2)_{max}} \right)^{1/2} \leq 1$$

Texture Aspect Ratio or S_{tr}

$$0 < S_{tr} = \frac{The\ length\ that\ the\ normalized\ AACF\ has\ the\ fastest\ decay\ to\ 0.2\ in\ any\ direction}{The\ length\ that\ the\ normalized\ AACF\ has\ the\ slowest\ decay\ to\ 0.2\ in\ any\ direction} \leq 1$$

Owing to the use of statistically superior autocorrelation functions in its definition, the S_{tr} is believed to be more accurate and reliable than the 1-D counterpart, γ.

The Areal Autocorrelation function (AACF) for the disk samples and steel pin are depicted in isometric plots shown in Figures 70 to 74. Notice each figure contains the AACF plots for virgin and worn states of each sample. Prior to the 2-D roughness analysis, it was anticipated that the surfaces would be strongly anisotropic, supported by the predominent texture directionality visualized in the earlier optical images. Indeed this seems to be the case; the S_{tr} for the surfaces are all less than 0.3, indicating a high degree of anisotropy. Notice also how the

texture directionality exhibited on the surface images are visually captured in the AACF plots as well. Since the disk surface images are only low-pass filtered, all the low frequency components are evidently well-preserved. On the contrary, the pin surface image is band-passed, hence the lack of low frequency features in its AACF plot.

A question arises as to whether the anisotropy becomes stronger or weaker as the surface goes through wear. As for ¼ and ½ T_{scuff} stages, the anisotropy became stronger shown by the reduction in the S_{tr} from their virgin to worn states. At ¾ scuffed stage, however, the gap between virgin and worn becomes almost unnoticeable. Finally at fully scuffed stage, the scuffed S_{tr} exceeds the virgin S_{tr} though not by much, possibly indicating its degenerating tendency of the anisotropy. When one is to observe mainly the S_{tr} values before and after wear within individual sample, an inevitable conclusion can be drawn. As the surface undergoes more wear, initial tendency towards stronger anisotropy lessens despite the obvious manufacturing variation among samples.
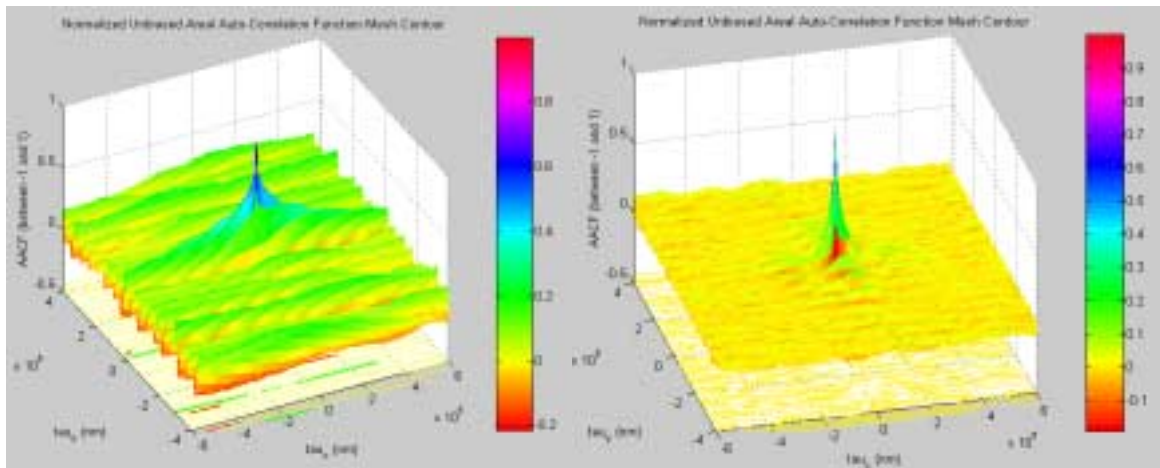

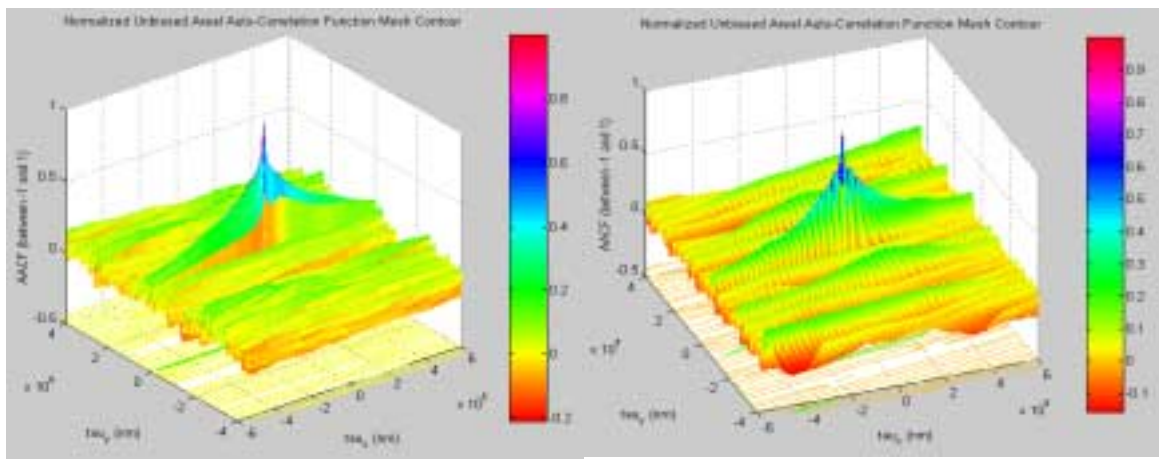Figure 27: AACF plots for Sample 2 – Virgin (left) and ¼ Scuffed (right) parts

Figure 28: AACF plots for Sample 3 – Virgin (left) and ½ Scuffed (right) parts
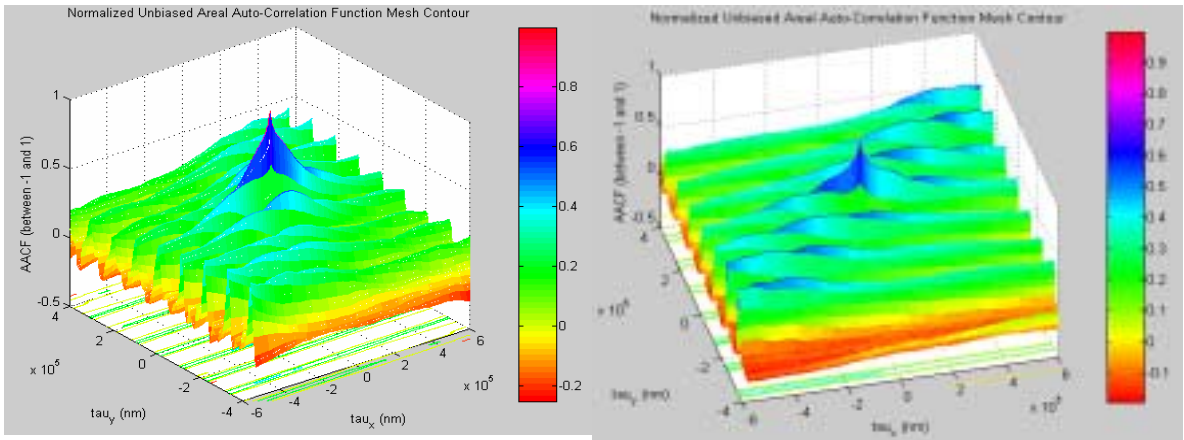
Figure 29: AACF plots for Sample 4 – Virgin (left) and ¾ Scuffed (right) parts
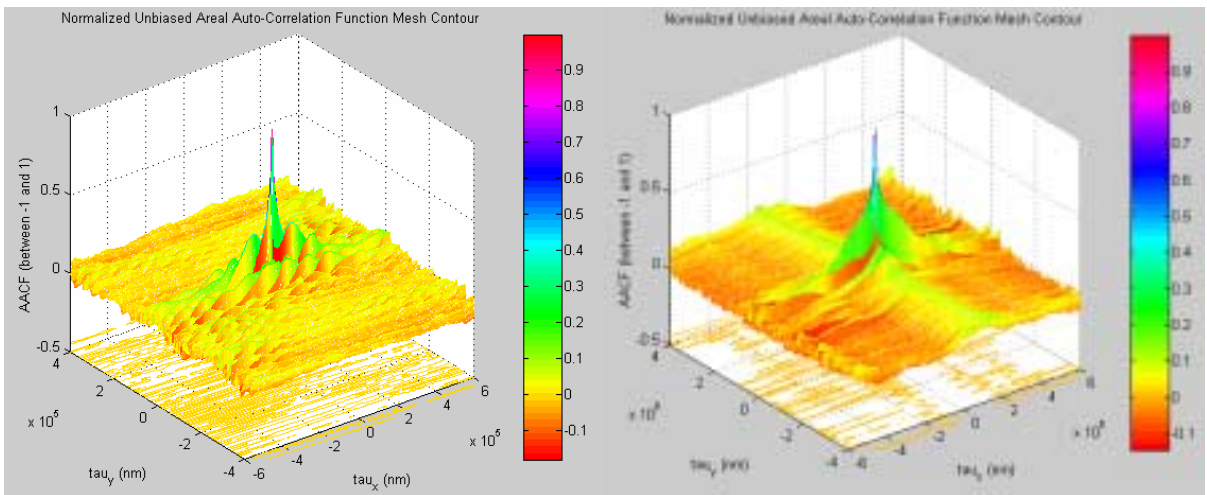
Figure 30: AACF plots for Sample 5 – Virgin (left) and Fully Scuffed (right) parts
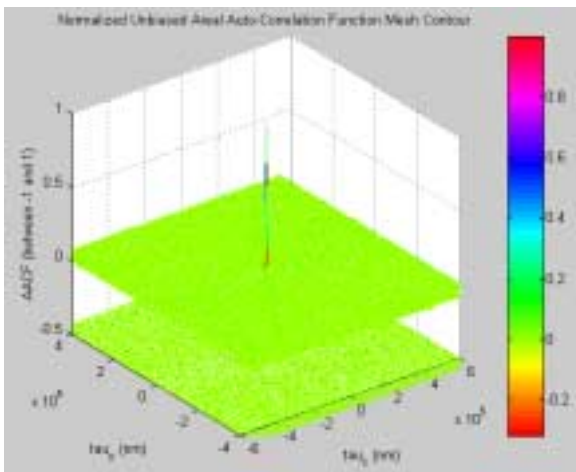
Figure 31: AACF plot for virgin steel pin

1.9.2.3 Areal Power Spectrum Density and $^7S_{td}$ (Texture Direction) Analysis

In order to determine the texture direction of the surface, first the Areal Power Spectrum Density (APSD) analysis, immediately followed by the angular spectrum analysis, must be performed (Stout *et al.*, 1993). Following the texture definition explained in Chapter 2, the lay directions are found to be the angle at which the maximum peak occurs in the angular spectrum matrix. Figure 75 reiterates the definition of texture direction determined by the APSD analysis, using the optical image of a worn part of Sample 3 or ½ T_{scuff} sample.
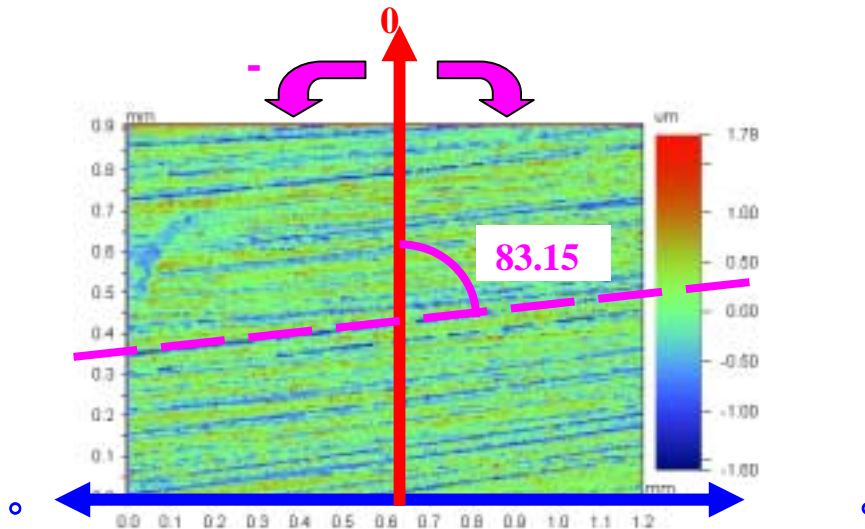
Figure 32: Texture direction defined by the APSD (Stout *et al.*, 1993)

The APSD matrix plot and the corresponding angular spectrum plot of all scuff and virgin stages are shown side by side in the following graphs, Figures 76 to 84. The lay direction is market in each angular spectrum plot. Notice while all the disk samples, whether virgin or worn, have a distinctive maximum peak in their angular spectrum plots, the pin sample does not.
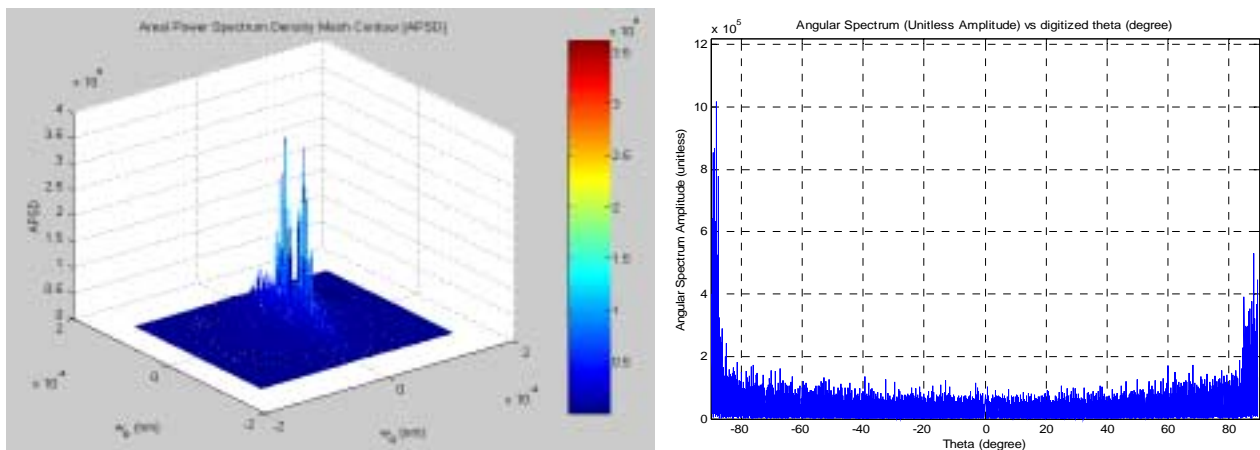
Figure 33: APSD (left) and $G_a(\theta)$ plots for Sample 2 – Virgin Part
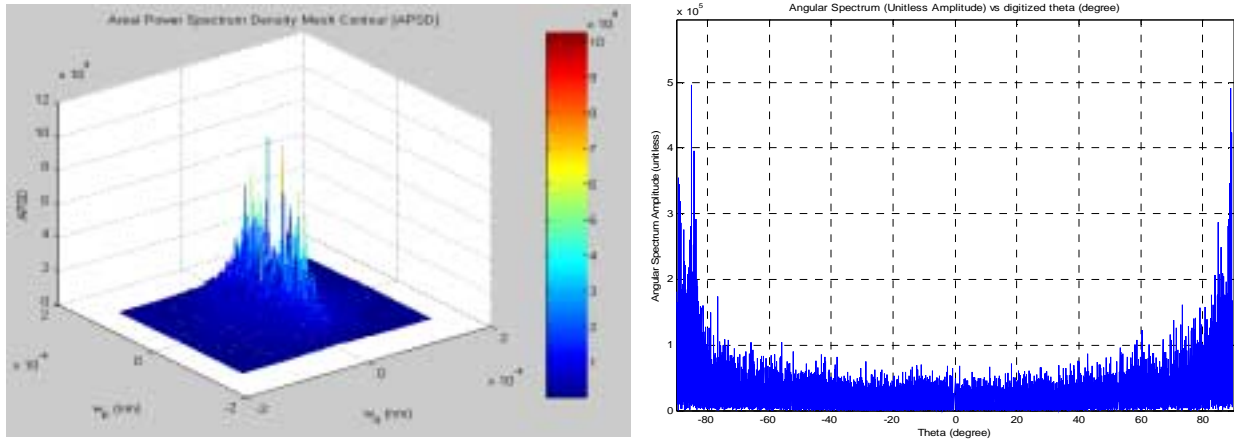
Figure 34: APSD (left) and $G_a(\theta)$ plots for Sample 2 – ¼ x T_{scuff} Part
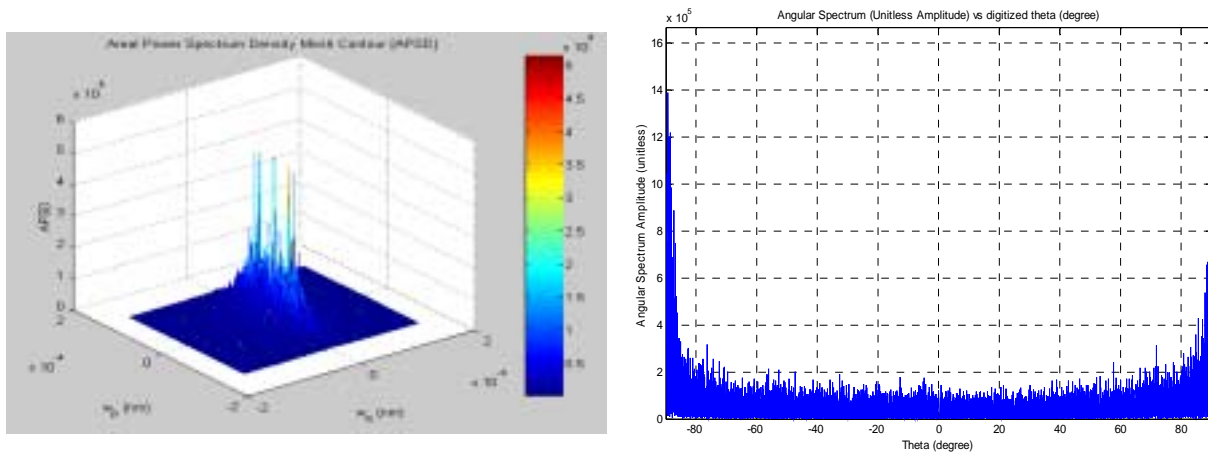
Figure 35: APSD (left) and $G_a(\theta)$ plots for Sample 3 – Virgin Part
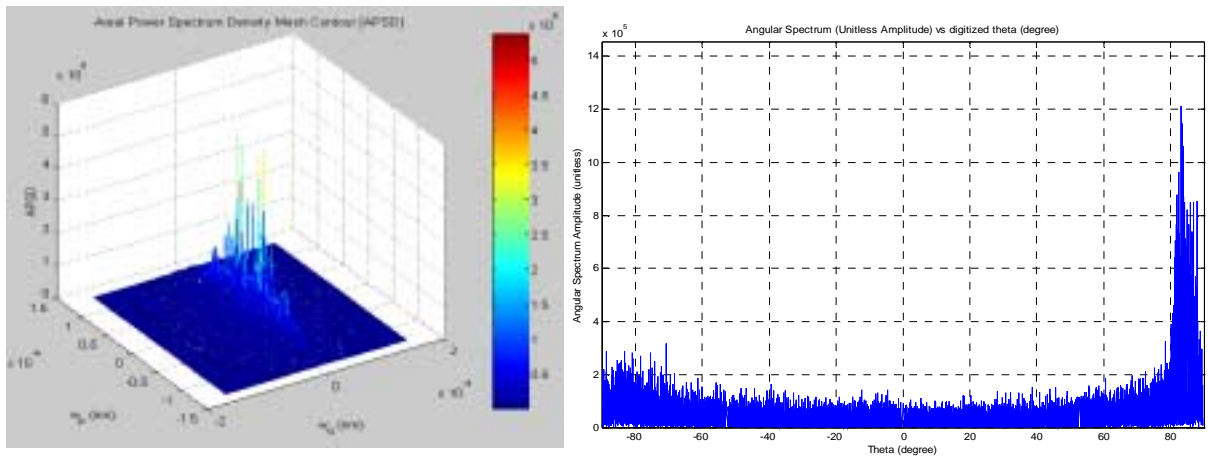
Figure 36: APSD (left) and $G_a(\theta)$ plots for Sample 3- ½ x T_{scuff} Part

31
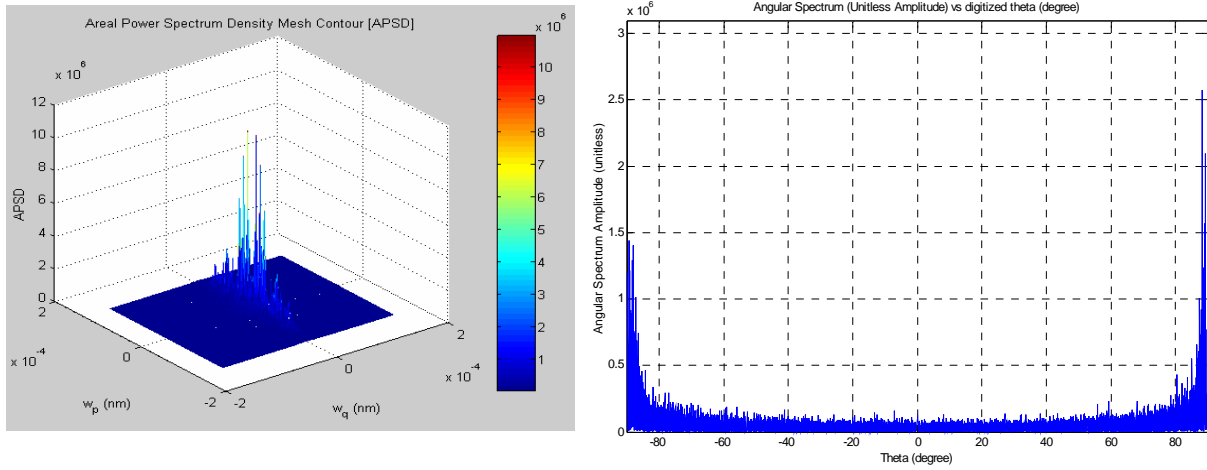
Figure 37: APSD (left) and $G_a(\theta)$ plots for Sample 4 – Virgin Part
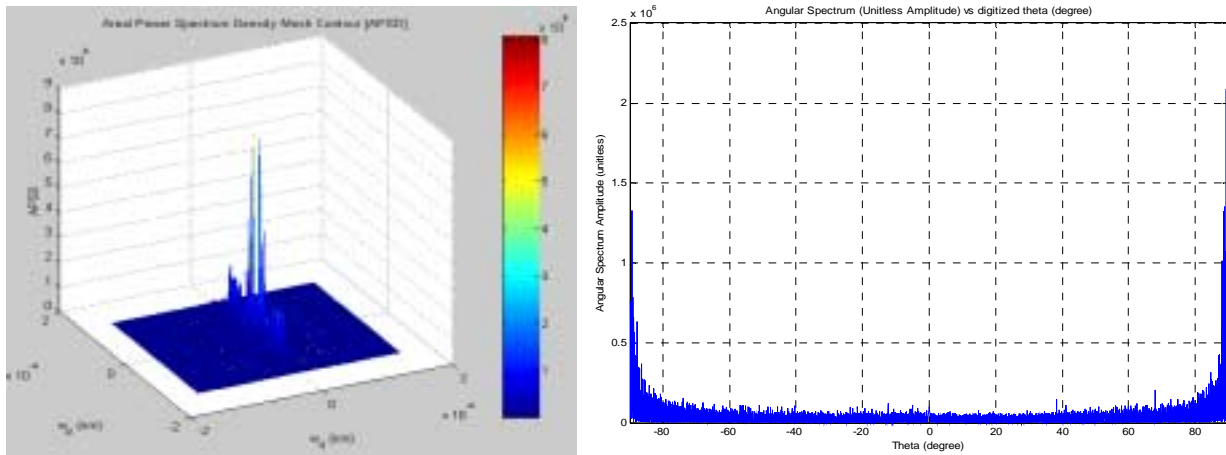
Figure 38: APSD (left) and $G_a(\theta)$ plots for Sample 4 – ¾ x T_{scuff} Part
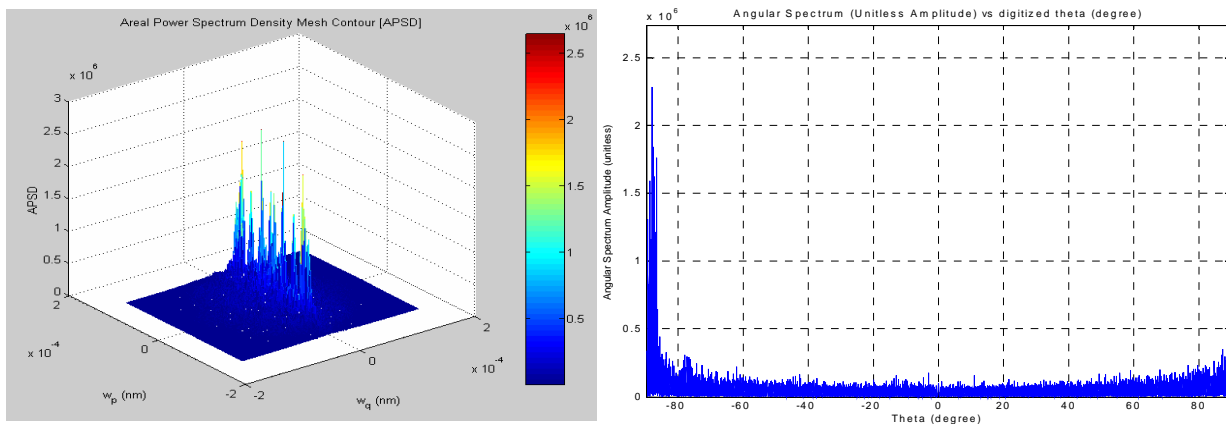
Figure 39: APSD (left) and $G_a(\theta)$ plots for Sample 5 – Virgin Part
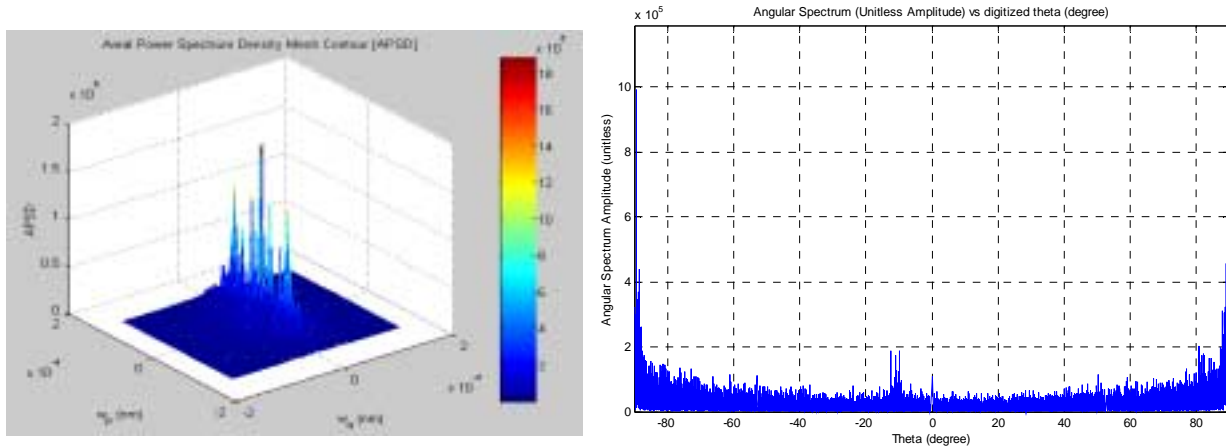
Figure 40: APSD (left) and $G_a(\theta)$ plots for Sample 5 – T_{scuff} Part
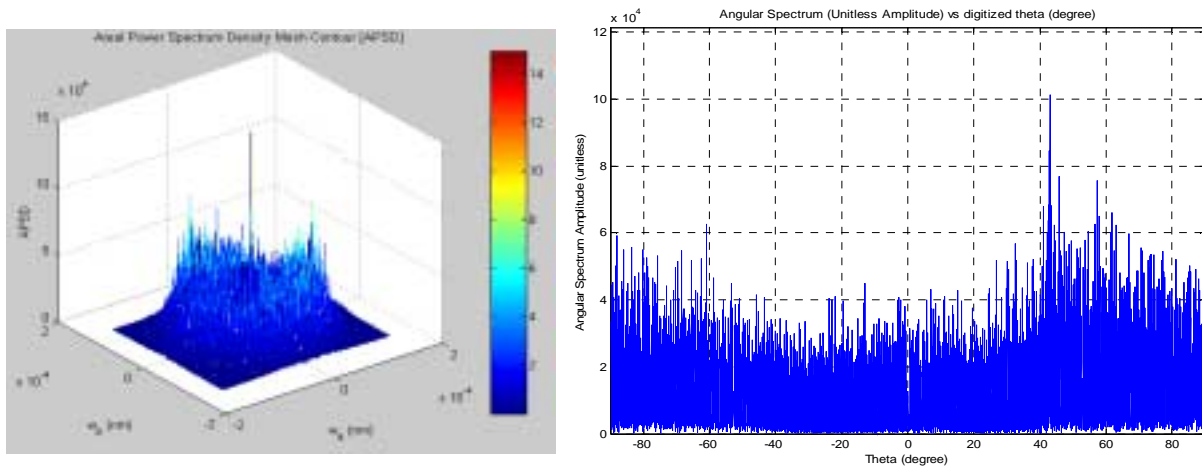
Figure 41: APSD (left) and $G_a(\theta)$ plots for Steel Pin

All the angular spectrum plot results agree with the visual observation of the optical images, exhibiting the most pronounced angular spectrums concentrated in the direction of lay. For the pin image, the lack of pronounced directionality in the APSD $G_a(\theta)$ plots is expected since its surface is determined to be highly isotropic by the earlier AACF study and S_{tr} value (1-D : γ=0.68, 2-D : $S_{tr} = 0.93$). By definition, the direction of the highest APSD value (also appears as the highest peak in $G_a(\theta)$ plot) is perpendicular to the direction of the actual surface lay.

1.9.2.4 [8]S_{al} (The Fastest Decay Correlation Length) Trends and Analysis

The fastest decay correlation length S_{al} is used to indicate whether the surface is dominated by low or high frequencies. The AACF tends to be greatly influenced by the choice of filtering methods and the corresponding cutoff frequencies. Since all the surfaces were treated with the same filtering scheme with the same sampling conditions, the inconsistencies related to filtering are minimal. Overall, the worn states possess far smaller S_{al} values than their virgin states, except for fully scuffed stage. However, due to the erratic nature at fully scuffed stage, this behavior can be ignored.
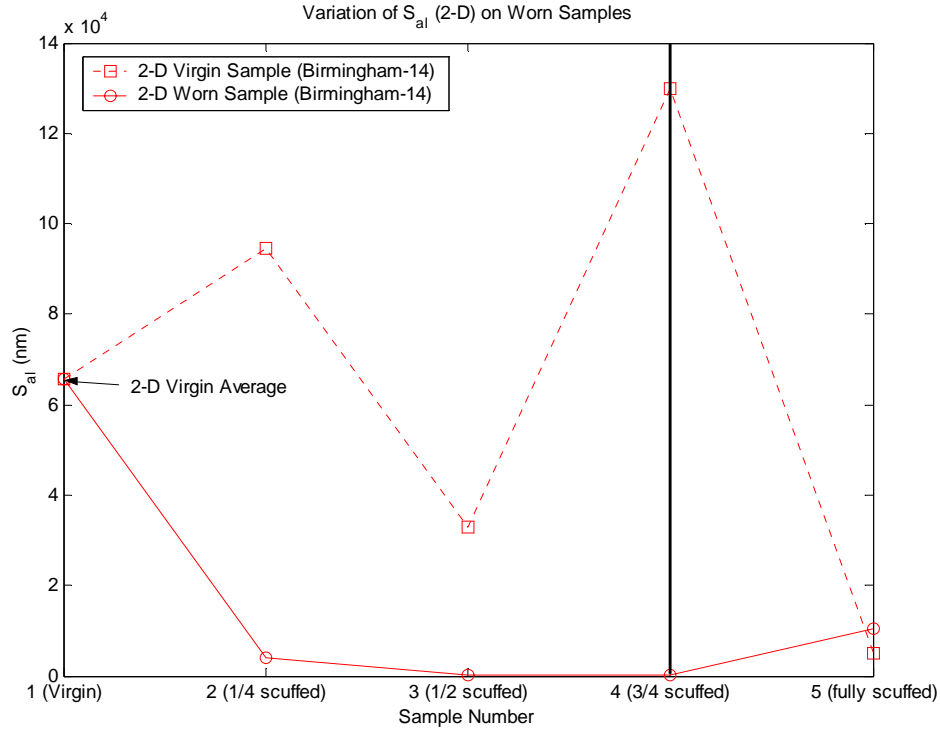
Figure 42: Variation of S_{al} (2-D) on worn samples

As for wear trend among disks, the S_{al} initially seems to decrease drastically from the ¼ scuffed to ½ scuffed stages. The large S_{al} value at ¼ scuffed stage indicates that surface is first dominated by low frequencies (long wavelength), but after undergoing more wear it becomes dominated by high frequencies (short wavelength), for instance at ½ and ¾ scuffed stages. However, when the surface is transformed to fully scuffed, the decreasing S_{al} trend is completely set off course by even surpassing the value at ¼ scuff time. Furthermore, at fully scuffed stage the S_{al} increases drastically from its virgin state as well, indicating that the surface is dominated by low frequency roughness components. Figure 85 summarizes the general trends of the S_{al} of the worn parts as the surfaces approaches scuffing. Also included in the figure is the S_{al} of the virgin parts, to enable direct comparison within the individual disk sample.

1.9.3 Hybrid Parameters for the Al390-T6 Samples

Hybrid parameters explain relative characteristics between amplitude and spatial properties. For instance, what is simply considered as the summit radius R or curvature by 1-D definition (i.e. line-profiles) can be expanded into the true 2-D perspective radius or curvature S_{sc}. The parameter S_{dr}, or developed interfacial area ratio, is a unique 2-D parameter and is worth investigating its trend. The RMS of summit curvature $S_{\Delta q}$ is another hybrid parameter developed from 1-D, which utilizes the user's chosen summit/valley definition. Each notation or parameter in Tables 19 and 20 stands for,

- $^9\mathbf{S_{\Delta q}}$ = Root-Mean-Square Slope of the Surface (Stout et al., 1993)
- $^{10}\mathbf{S_{sc}}$ = Arithmetic Mean Summit Curvature of the Surface (Stout et al., 1993)

34

- κ_e = Equivalent Isotropic Mean Summit Curvature (McCool, 1986)
- R_e = Equivalent Isotropic Radius of Spherical Summits (McCool, 1986)
- [11]S_{dr} = Developed Interfacial Area Ratio (Stout et al., 1993)

Table 8: Hybrid parameters of virgin Samples (2-5) and steel pin

Hybrid Parameters		Virgin Parts/Samples				
		Sample 2	Sample 3	Sample 4	Sample 5	Pin
[9]$S_{\Delta q}$ (no units)	B-14	0.078	0.14	0.16	0.12	0.023
[10]S_{sc} (µm^{-1})	B-14	0.028	0.049	0.049	0.041	0.0090
κ_e or R_e^{-1} (µm^{-1})	SM-EI-2D	0.025	0.040	0.038	0.036	0.0093
	SM-EI-1D	0.097	0.119	0.140	0.113	
S_{sc}^{-1} (µm)	B-14	35.21	20.92	20.24	24.27	111.69
R_e (µm)	SM-EI-2D	39.89	24.75	26.18	28.19	108.09
	SM-EI-1D	10.29	8.42	7.15	8.85	NA
[11]S_{dr} (%)	B-14	0.30	1.00	1.19	0.67	0.027

Table 9: Hybrid parameters of worn Samples (2-5)

Hybrid Parameters		Sample 2	Sample 3	Sample 4	Sample 5
		¼ Scuffed	½ Scuffed	¾ cuffed	Fully Scuffed
[9]$S_{\Delta q}$	B-14	0.058	0.12	0.10	0.065
[10]S_{sc} (µm^{-1})	B-14	0.020	0.040	0.024	0.018
κ_e or R_e^{-1} (µm^{-1})	SM-EI-2D	0.019	0.035	0.026	0.020
	SM-EI-1D	0.054	0.090	0.116	0.031
S_{sc}^{-1} (µm)	B-14	50.16	25.04	42.35	54.44
R_e (µm)	SM-EI-2D	53.08	28.40	38.66	51.35
	SM-EI-1D	18.39	11.08	8.58	32.84
[11]S_{dr} (%)	B-14	0.17	0.75	0.49	0.21

1.9.3.1 [9]$S_{\Delta q}$ (Root-Mean-Square of the Surface) Trends and Analysis

The hybrid slope $S_{\Delta q}$ is the scalar magnitude of the continuous surface slope at any point, computed by calculating *x*- and *y*- components separately as for a line-profiles. The $S_{\Delta q}$ or the RMS values of the surface slope within the sampling area of the Al390-T6 disks have a decreasing trend as the surface wears to full scuffing. The reason for the decreasing trend can be again accredited to the intensified polishing of the top portion of asperities, thereby reducing the total RMS of asperity slope with more wear. The sudden increase in the worn $S_{\Delta q}$ from ¼ scuffed to ½ scuffed is perhaps due to the manufacturing variation inherent in their virgin samples. Because the virgin sample variation is more prominent in the $S_{\Delta q}$ analysis than in other parameters, wear evolution through

different scuffing stages is difficult to substantiate. Instead, the amount of change in the $S_{\Delta q}$ from virgin to worn states at each scuffing time may yield some worthwhile wear evolutionary behavior. As it appears in Figure 86, all the worn $S_{\Delta q}$ values are lower than the virgin $S_{\Delta q}$ values because of the burnished asperities. The difference between worn $S_{\Delta q}$ and virgin $S_{\Delta q}$, however, seems to increase for more severely worn stages, i.e. ¾ scuffed and fully scuffed. This indicates that the $S_{\Delta q}$ decreases steadily with respect to wear. This result seems to agree with the previously regarded asperity-polishing observation, in which the slope of a summit is expected to reduce when the top asperity is worn off.
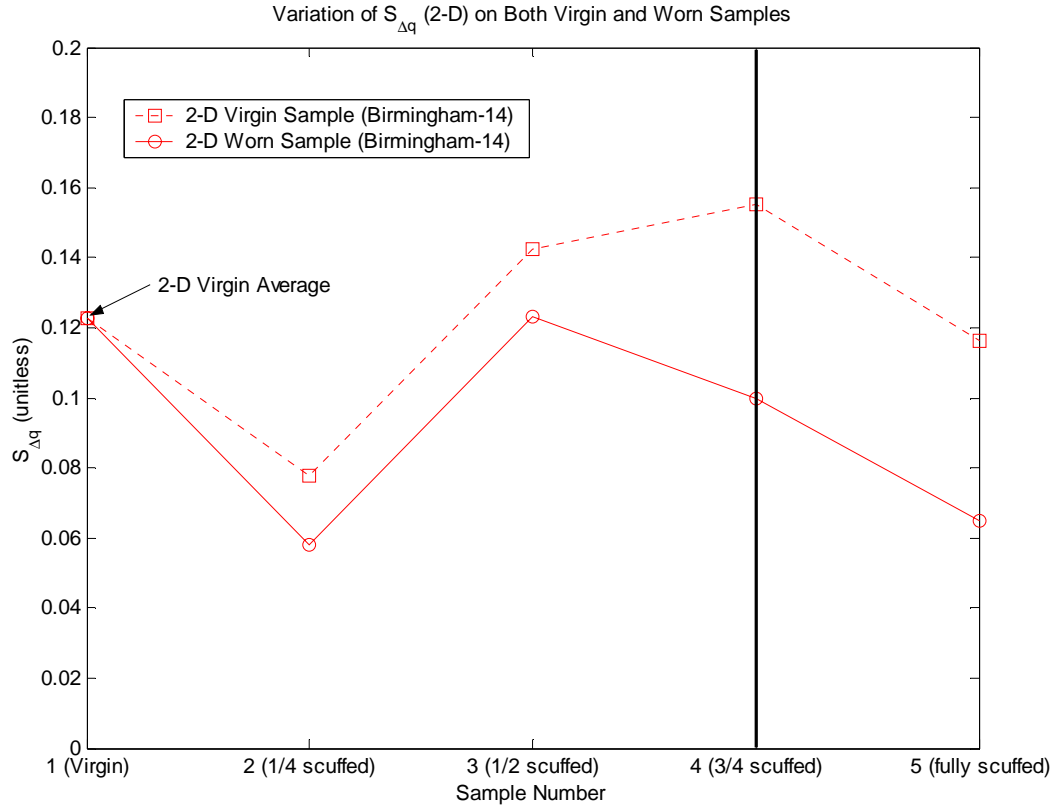
Figure 43: Variation of $S_{\Delta q}$ (2-D) on virgin and worn samples

1.9.3.2 R or S_{sc}^{-1} (Arithmetic Mean Summit Radius) Trends and Analysis

Recall that the mean summit curvature (i.e. κ) and radius (i.e. R) are inversely related according to the spectral moment roughness characterization (McCool, 1986). The Birmingham-14 equivalent κ is the S_{sc}, while the mean summit radius is not defined in the Birmingham standards. Since the R (i.e. the average radius of curvature of asperities, or simply asperity radius) is easier to visualize conceptually, change in the R rather than in the S_{sc} is observed ($R = 1/S_{sc}$). The worn R exhibits an increasing trend, with an exception of a sudden plunge at ½ scuffed stage. The erratic behavior of the worn R at ½ scuffed time agrees with the sudden increase at this stage found in the previous $S_{\Delta q}$ trend, which may have been caused by disk-to-disk variation. The same irregularity at ½ scuffed time has been observed in the earlier $S_{\Delta q}$ analysis, i.e. sudden increase in the $S_{\Delta q}$. This seems to indicate that the R and

$S_{\Delta q}$ (RMS slope) are in cause-and-effect relationship; the larger the asperity radius, the larger the RMS slope, or vice versa. Overall, the sample-to-sample variation in the virgin R is comparably small.

As for the individual sample, wear increases the asperity radius. A simple explanation for this is once again the burnishing of the asperities due to wear, eventually leading to larger radii of curvature. The difference between the virgin R and worn R from sample to sample also increases progressively, reaching its highest at fully scuffed time. This observation agrees with the asperity wear-polishing theory previously defended. In hindsight, the progression in wear should reveal more (previously not recognized) asperities populated in the lower zones. By the time of full scuffing, however, the smaller asperities have undergone severe plastic deformation, thus have very little statistical contribution to the total summit radius calculation.
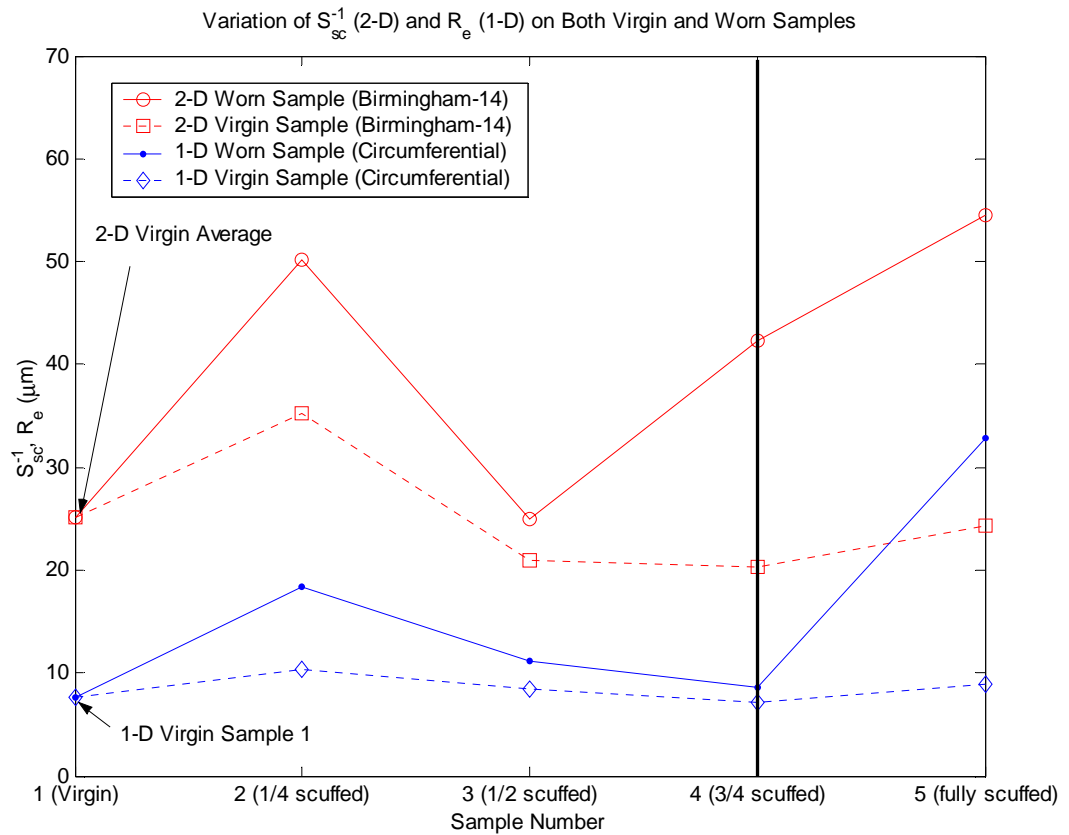
Figure 44: Variation of S_{sc}^{-1} (2-D) and R_e (1-D) on virgin and worn samples
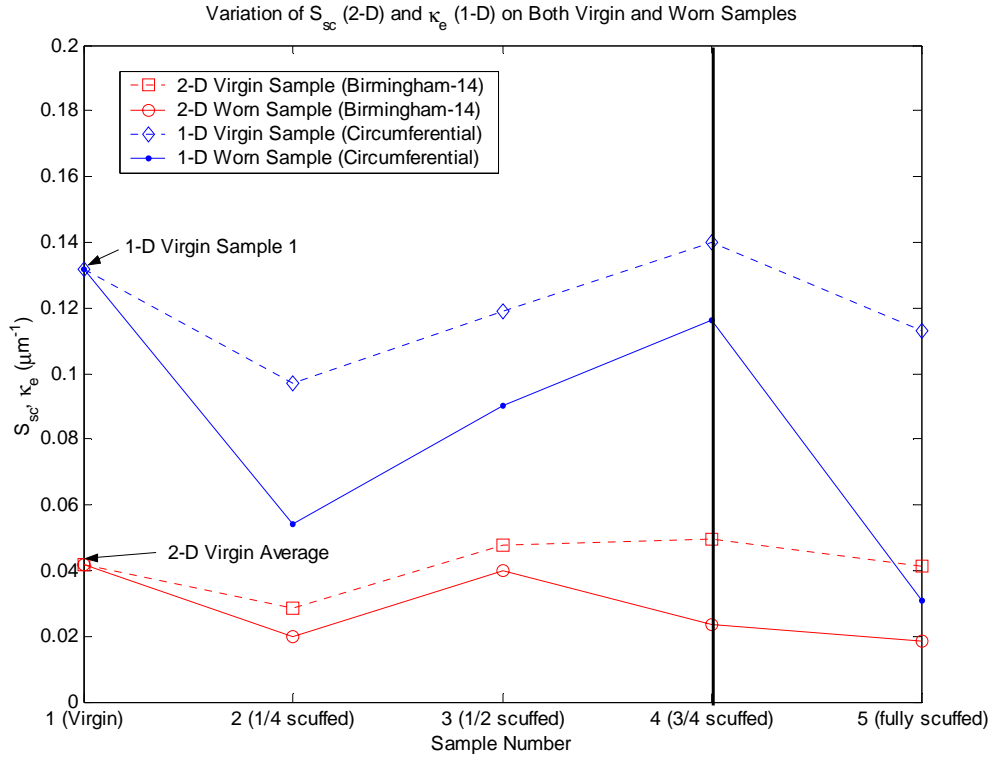
Figure 45: Variation of $\underline{S}_{sc}$ (2-D) and κ_e (1-D) on virgin and worn samples

1.9.3.3 [11]S_{dr} Trends and Analysis

The trend in the developed area ratio S_{dr} can further enhance the understanding of the geometric evolution of wear-polished asperities. S_{dr} stands for the unique 2-D measure of how much the true area of the surface exceeds that of the nominal reference surface, i.e.

$$S_{dr} = \frac{\overbrace{Total\ Surface\ Area - Sampling\ Area}^{Areal\ Difference}}{Sampling\ Area} \cdot 100\%$$

With an exception of ¼ T_{scuff}, the general trend of the S_{dr} is that as the surface is worn out, the S_{dr} decreases, indicating that the real surface area decreases. This fits the intuition where one would naturally expect less surface area when more asperities are sheared and knocked out due to damaging contact. As for individual virgin to worn states, the worn S_{dr} is always smaller than the virgin and their difference increases with more wear. The conclusion from Figure 89 is that the true surface area existing above the mean plane diminishes with wear.

Notice how the trend of the S_{dr} is very similar to those of the amplitude properties (e.g. S_a and S_q), and other hybrid parameters ($S_{\Delta q}$ and S_{sc}); [1]values for worn parts are always lower than virgin parts, [2]values for worn parts always increasing at ½ scuffed than decreasing till fully scuffed. When compared to the published values of other engineering surfaces, the S_{dr} values of the Al390-T6 samples are relatively large, though the sampling conditions are different (Stout *et al.*, 1993). Table 21 summarizes the various existing manufactured surfaces for easy comparison.

Table 10: S_{dr} (%) comparison between the published values and scuffing experiments (Stout *et al.*, 1993)

Published Values [Stout, 1993]		
	(Δx, Δy)	S_{dr} (%)
Ground	(8 μm, 8 μm)	0.314
	(16 μm, 16 μm)	0.112
Polished	(3.75 μm, 3.75 μm)	0.0086
	(7.5 μm, 7.5 μm)	0.0032
Honed	(10 μm, 10 μm)	0.178
	(20 μm, 20 μm)	0.074
Al390-T6 Experimental Values		
¼ Scuffed	(3.260 μm, 3.804 μm)	0.167
½ Scuffed	(3.260 μm, 3.804 μm)	0.752
¾ Scuffed	(3.260 μm, 3.804 μm)	0.491
Fully Scuffed	(3.260 μm, 3.804 μm)	0.210

The fact that the S_{dr} trend imitates the amplitude parameters indicates that these surfaces are significantly influenced by the amplitude characteristics. Although the S_{dr} graphs do not reveal any new behaviors, its result is consistent with the other parameters, further supporting the wear evolution of asperities of the surface.
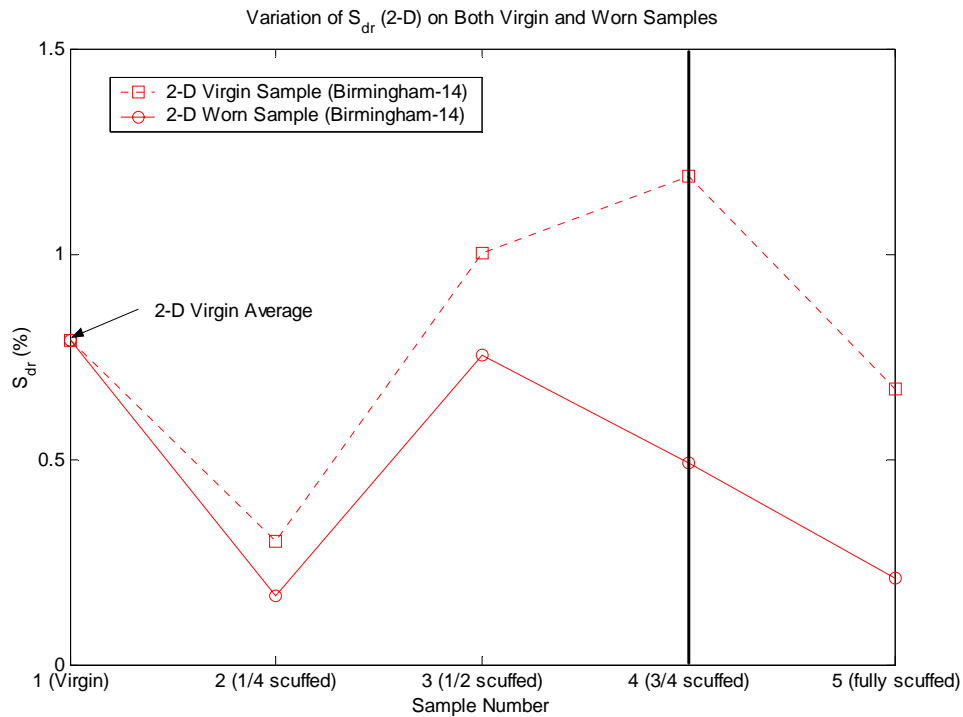
Figure 46: Variation of S_{dr} (2-D) on virgin and worn samples

1.9.4 Functional Parameters for the Al390-T6 Samples (Birmingham-14 only)

The 2-D surface topography influences not only the "mechanical and physical" properties of contacting interfaces, but also other "non-contacting" properties as well, such as functional applications (Dong *et al.*, 1994). The geometry property, i.e. amplitude and spatial properties, of a given 2-D surface topography changes wear,

friction, lubrication, and bearing of the surface, which affect performance and reliability of the component. Tables 22 and 23 summarize both volumetric and areal aspect of functional parameters of the Al390-T6 disk samples, all of which are derived from surface bearing area ratio curve provided in Figures 90 through 94. Truncation plane marks at 5 % and 80 % of bearing area are also included in the figures to categorize the bearing area into three functional zones, namely, material volume in peak zone, void volume in core zone, and void volume in valley zone

Table 11: Functional parameters of virgin Samples (2-5) and steel pin

3-D Functional Parameters		Virgin Parts/Samples				
		Sample 2	Sample 3	Sample 4	Sample 5	Pin
Volume (nm^3/nm^2)	S_m	11.12	20.68	23.17	14.04	3.18
	S_c	307.38	530.26	636.50	341.50	46.30
	S_v	31.12	58.83	79.15	40.68	6.67
(Bearing) Area	[12]S_{bi}	0.640	0.624	0.649	0.652	0.675
	[13]S_{ci}	1.462	1.492	1.422	1.422	1.376
	[14]S_{vi}	0.119	0.130	0.140	0.133	0.143

Table 12: Functional parameters of worn Samples (2-5)

3-D Functional Parameters		Sample 2	Sample 3	Sample 4	Sample 5
		¼ Scuffed	½ Scuffed	¾ Scuffed	Fully Scuffed
Volume (nm^3/nm^2)	S_m	8.736	10.787	8.858	8.049
	S_c	140.979	448.846	188.831	173.975
	S_v	25.156	51.208	84.282	35.170
(Bearing) Area	[12]S_{bi}	0.703	0.715	1.104	0.724
	[13]S_{ci}	1.285	1.286	0.681	1.214
	[14]S_{vi}	0.166	0.126	0.238	0.186

where

- S_m = Material Volume Ratio of the Surface from 0 % to 10 % of Bearing Area (Sacerdotti, 1996)
- S_c = Void Volume Ratio of the Surface from 10 % to 80 % of Bearing Area (Sacerdotti, 1996)
- S_v = Void Volume Ratio of the Surface from 80 % to 100 % of Bearing Area (Sacerdotti, 1996)
- [12]S_{bi} = Surface Bearing Index or the Ratio between the S_q and the Surface Height at 5 % of Bearing Area (Stout et al., 1993)
- [13]S_{ci} = Core Fluid Retention Index or the Ratio between the Void Volume of the Unit Sampling Area at the Core Zone (5 % - 80 % of BA) over the S_q (Stout et al., 1993)
- [14]S_{vi} = Valley Fluid Retention Index or the Ratio between the Void Volume of the Unit Sampling Area at the Valley Zone (80 % - 100 % of BA) over the S_q (Stout et al., 1993)

As for worn to wear variation shown in Figure 90, each worn stage is hardly distinguishable from one another with no apparent relationship. The main reason for the lack of variation among the worn samples is perhaps due to normalization embedded in the h to enable relative comparison. Each y-axis or the truncation height is

normalized with respect to its own S_q of each disk, making the difference hardly noticeable. Another reason for the lack of trends in the bearing area ratio curve may be due to the initial disk-to-disk variation. Since a significant amount of variability was present in the initial samples due to manufacture irregularities, any entitled modification on the bearing area may have been lost, creating somewhat of the zero-sum phenomena. If the scuffing test had been done on the same sample progressively and the surface topography at each stage had been recorded, there may have been much more variation in their bearing areas.
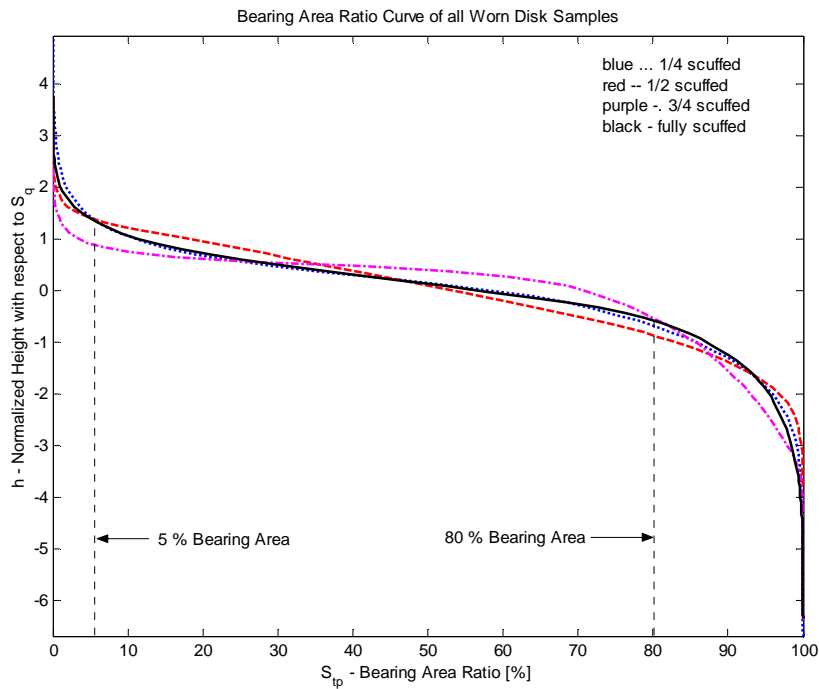

Figure 47: Bearing area ratio curves for all worn disk samples

Much can be observed in the bearing area ratio curves (Figures 91 to 94) all of which show virgin and worn states overlaid together. Again, the difference between virgin and worn parts is hardly recognizable except at ¾ scuffed time. The dramatic difference at ¾ scuffed time in Figure 93 may be due to increasingly detrimental plastic deformation in the asperities as the contact-sliding wear approaches fully scuffed stage. At the fully scuffed stage, however, the lack of variability between virgin and scuffed may seem questionable at first glance (Figure 94). However, a transfer of material between the Al390-T6 disk and 52100 steel pin at scuffing may have well resulted in a null change in the total bearing area. At the same time, one must also keep in mind that at full scuffing the damage may be highly localized effects by varying irregularly, since the surface has become highly unstable and non-uniform at the time of scuffing. Furthermore, the width of scuffing track varies up to 8 mm, while the prescribed scan are that can be captured by Wyko optics is only about 1.2 mm by 0.9 mm. The way to remedy this is to obtain a larger scan image with, for instance, a 2-D contact profilometer.
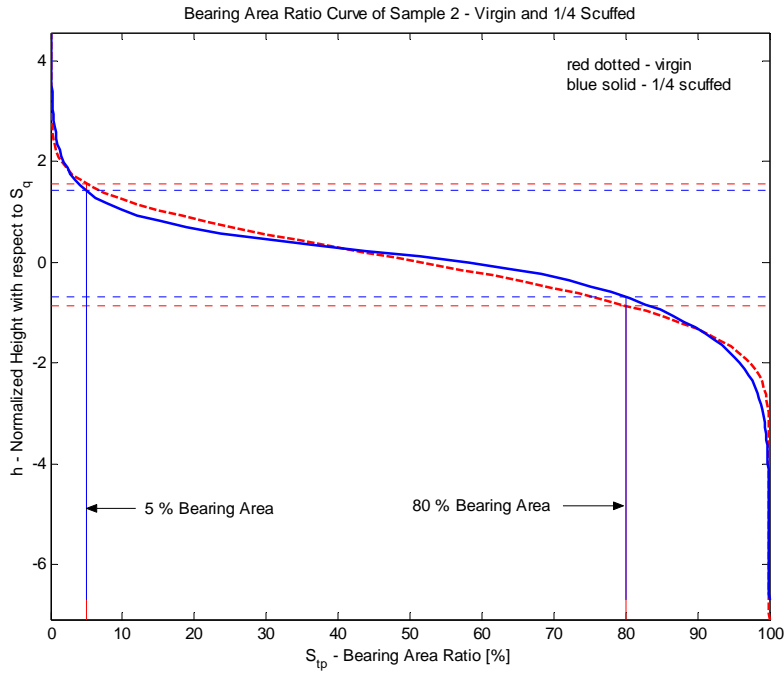
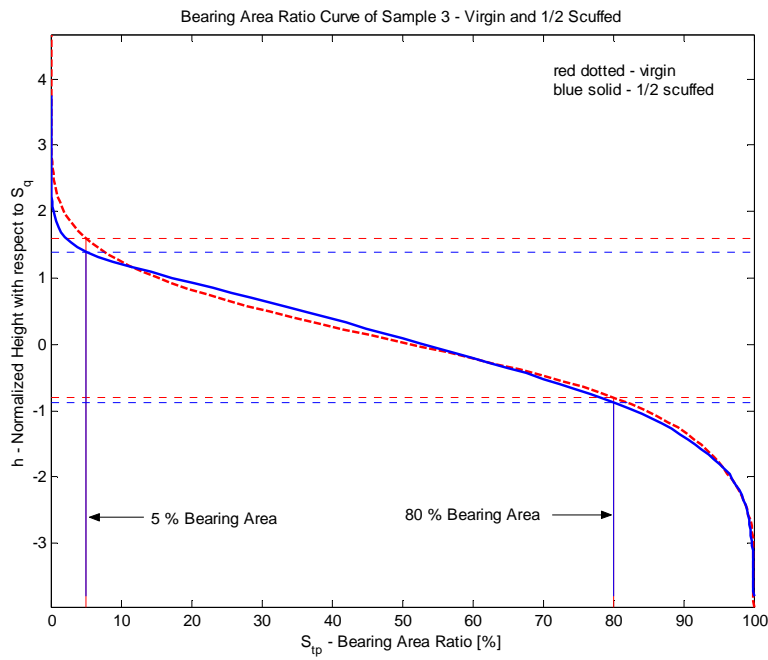Figure 48: Bearing area ratio curve for Sample 2 – Virgin and ¼ x T_{scuff} Parts

Figure 49: Bearing area ratio curve for Sample 3 – Virgin and ½ x T_{scuff} Parts
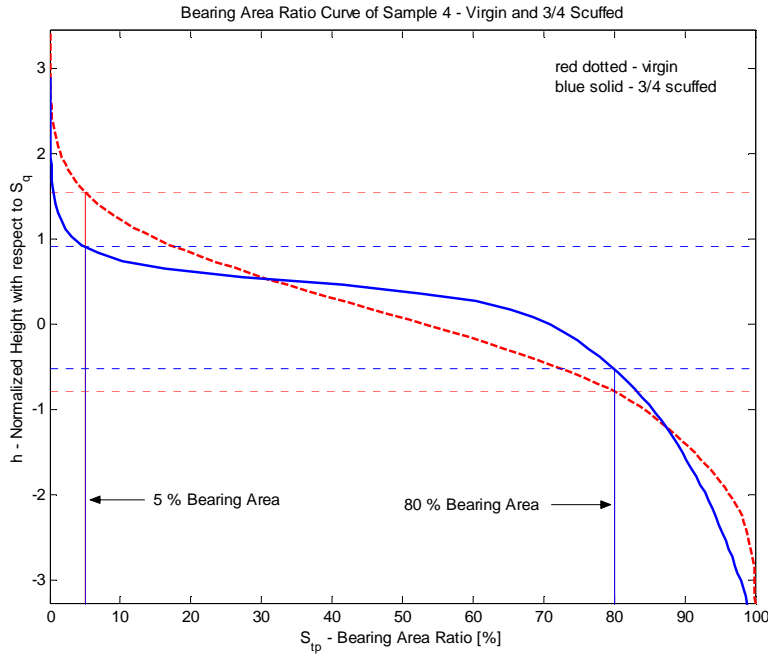
Figure 50: Bearing area ratio curve for Sample 3 – Virgin and ¾ x *T~scuff~* Parts
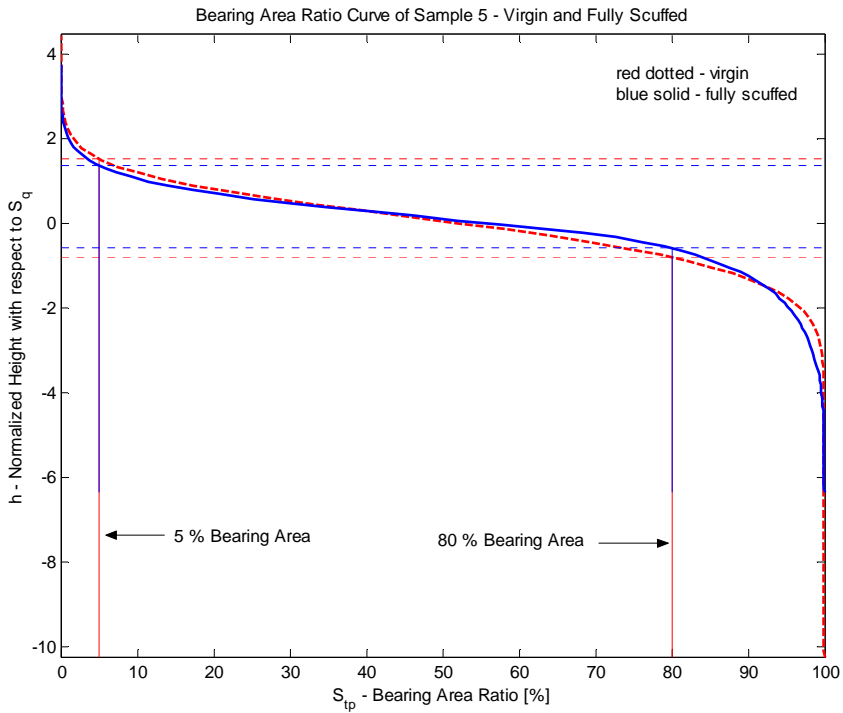

Figure 51: Bearing area ratio curve for Sample 5 – Virgin and *T~scuff~* Parts

- Areal Functional Parameter Trends and Analysis

Rather than analyzing the functional characteristics of the disks in terms of "absolute physical quantities" presented in bearing area ratio curve which is not only qualitative but also can get easily complicated, using a series of simple indexes is a simpler and better method. As summarized in Tables 22 and 23, three functional indexes derived from the bearing area curves describe the functional evolution of the Al390-T6 disks with wear. They are, surface bearing index (S_{bi}), core fluid retention index (S_{ci}), and valley fluid retention index (y), all of which are drawn from the horizontal intersections at 5 % and 80 % bearing area.

1.9.4.1 S_{bi} Trends and Analysis

By definition, S_{bi} is the ratio of the S_q over the surface height at 5 % bearing area $h_{0.05}$. Although the bearing area ratio curve for each worn stage does not show much physical difference, marked differences are shown when analyzed in terms of S_{bi}. One novel advantage in doing this analysis is that the S_{bi} values for virgin parts stay nearly constant and very Gaussian (≈ 0.608). This immediately eliminates the issues concerning disk-to-disk variation. As for individual worn stage, worn S_{bi} values are always higher than virgin S_{bi} values. An increase in S_{bi} is expected when undergoing wear, as it was reported that as the surface is worn out, the S_{bi} value grows from Gaussian 0.608 (Stout *et al.*, 1993). As for the global trend, the S_{bi} increases as well. If the fully scuffed stage is ignored, the worn S_{bi} graph steadily increases, peaking its highest just before scuffing. Generally, the higher the S_{bi}, the better the bearing property of the surface. If only the S_{bi} is considered ignoring other roughness properties, chemical and micro-structural properties, the bearing property of the Al390-T6 disk increases as the surface undergoes wear.
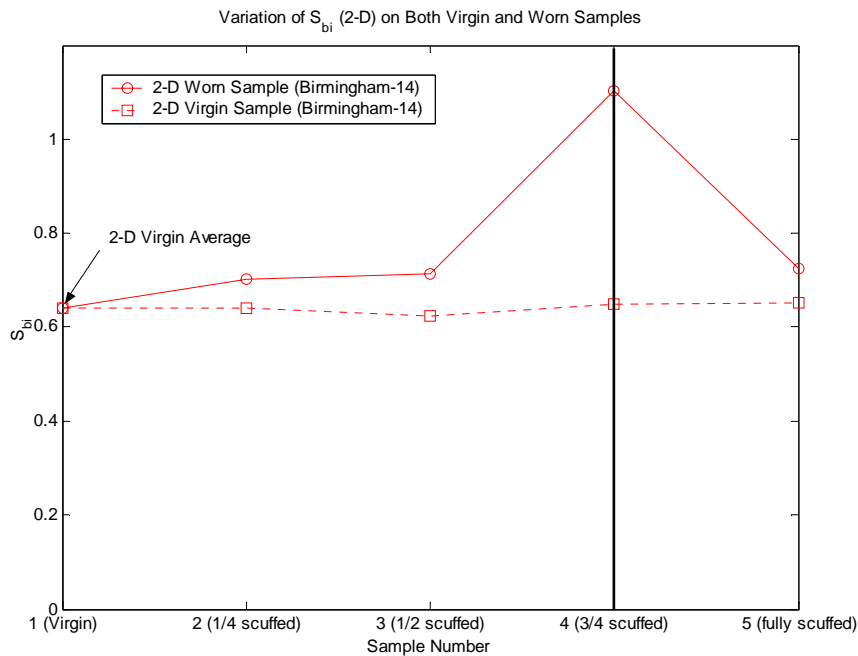

Figure 52: Variation of S_{bi} (2-D) on virgin and worn samples

1.9.4.2 S_{ci} Trends and Analysis

S_{ci} is the ratio of the void volume at the core zone defined by 5 % ~ 80 % bearing area. The void area trapped in this zone is integrated using the trapezoidal rule (see APPENDIX C), and normalized with respect to the

sampling area and the S_q. Similar to the S_{bi} trend, all virgin parts are approximately constant and near Gaussian ($\approx$ 1.56). Invariability in the virgin S_{ci} trend despite manufacturing irregularity makes this parameter not only unique but also reliable. In general, as a surface experiences wear, the S_{ci} decreases. Indeed for all the Al390-T6 samples, worn S_{ci} values are smaller than virgin S_{ci} values, showing signs of wear. As for moving through wear stages until just before fully-scuffed, the trend in the S_{ci} is decreasing, which is expected in a progressive wear. The scuffed stage should not be included in establishing a trend, due to its unpredictable nature of its state. The decreasing trend of the S_{ci} implies the deterioration of the fluid retention property in the core zone. This is a justifiable conclusion, since polishing of asperities inevitably decreases the void volume once formed by then existing asperities. Therefore, at scuffing fluid cannot be retained. From the S_{ci} graph, it is concluded that lubrication/refrigerant retention capability within the disk surface degenerates as the surface approaches full scuffing.
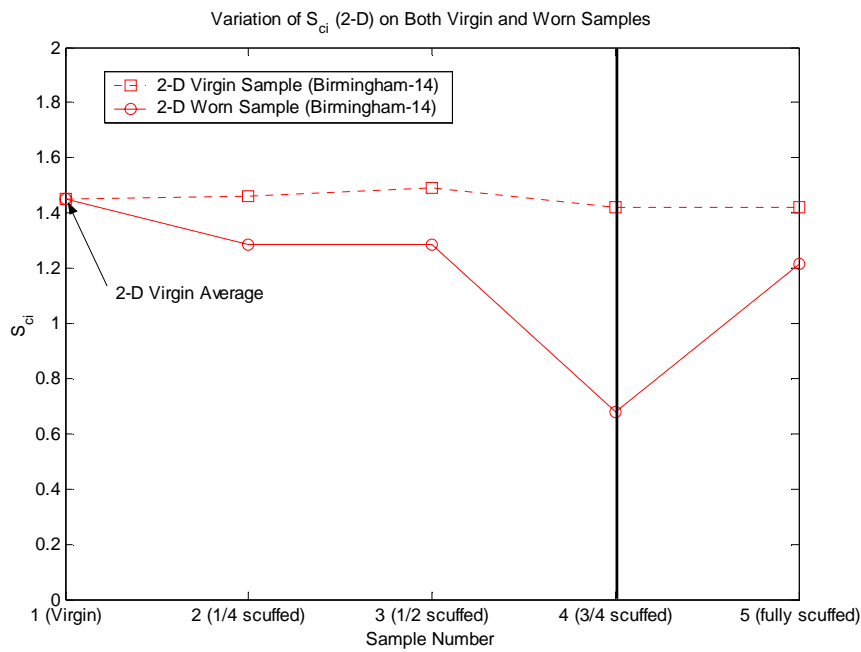

Figure 53: Variation of S_{ci} (2-D) on virgin and worn samples

1.9.4.3 S_{vi} Trends and Analysis

Similar to S_{bi}, S_{vi} is the ratio of the void volume at the valley zone entrapped within 80 % ~ 100 % bearing area. The void volume at this zone is calculated by integrating the bearing area within this range, and normalize the result by the sampling area and the S_q. Unlike the previous indexes, the S_{vi} is relatively constant for reasonable wear. If a value is significantly larger than 0.11, this indicates a flat top, which is deviated a form from a standard Gaussian distribution. From Figure 97, virgin S_{vi} appears to be relatively stable. For all wear stages except at ½ scuffed, worn S_{vi} values are larger, indicating its tendency towards a flatter surface geometry due to the wear process. The sudden decrease at ½ scuffed time, however, may be considered negligible, since the range of y-axis is very narrow. Overall, the trend in the S_{vi} may be perceived as increasing, the opposite of the S_{ci}. A reasonable explanation for this behavior is that as the surface progressively is worn out, the core void volume decreases while

the valley void volume increases in turn to compensate for the loss. However, the increase in the valley zone is usually not sufficient for full compensation, hence the reduction in the total fluid retention potential.
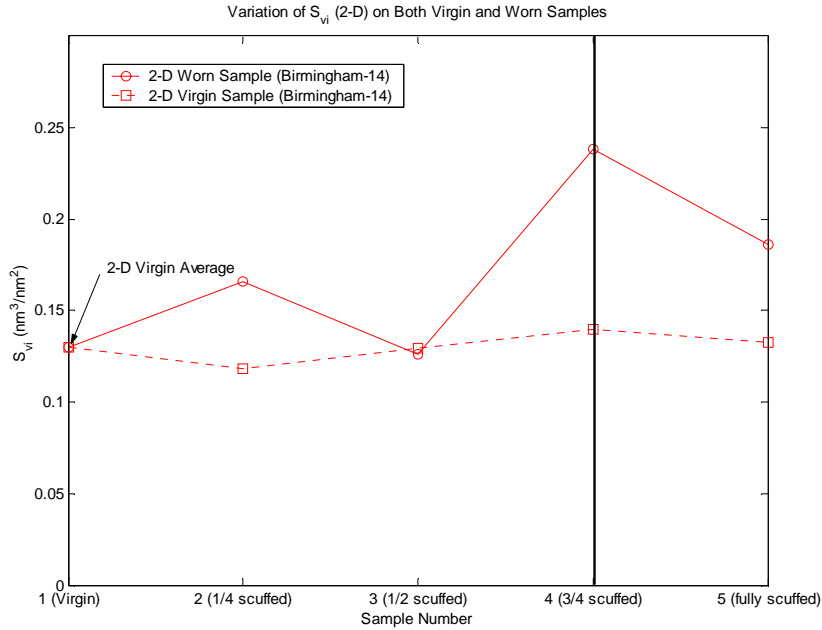

Figure 54: Variation of S_{vi} (2-D) on virgin and worn samples

1.10 Summary and Recommendations

In this chapter, the study of the wear evolution of the disk-pin contact prior to scuffing involved the use of the established surface topography characterization tools, namely the 2-D "Birmingham-14 parameters". Although a few primary roughness parameters had been investigated previously using the 1-D spectral moment computations (i.e. R_a, R_q, D_{summit}, R, R_{sk}, and R_{ku}), the study was not nearly comprehensive or thorough other than indicating that the surface topography has a "vital role" in scuffing (Patel, 2001). This is due to the lack of information implied in the 1-D line-profiles analysis, less viable statistically to the 2-D areal analysis. In this work, the Wyko non-contact optical imaging technique was adopted to obtain 2-D topographic data, instead of the Dektak 1-D contact profilometer used in the previous analysis. Based on the new 2-D optical data, various geometric and functional aspects of roughness characterization have been introduced, which are the least number of fundamental properties required to describe the 2-D surface topography. The novelty in the use of the "Birmingham-14" parameters in this study is that not only does it yield the numerically distinctive and statistically sound parameters, but more so that the roughness parameters at different wear stages prior to scuffing can be summarized simultaneously for practical comparison and trend analysis. The 2-D parameters are also directly compared to the 1-D parameters, in terms of their numerical values and trends. Despite the newly introduced parameters, it is found that the amplitude parameters in 1-D and 2-D are not significantly different in their trends in conjunction to wear. The spatial parameters and hybrid parameters furthermore support the hypothesis that as the virgin surface experiences more wear, the top asperities are smoothened out till scuffing, the conclusion solely based on geometry. However, it is in the functional parameters or indexes based on the bearing area curve, such as the S_{bi} and S_{ci} coefficients, that one can

draw a sound conclusion; unlike the other parameters, the functional indexes remain fairly constant in original state, making the inherent but dominant disk-to-disk variation minimal. In summary, in order to understand the effects of scuffing on the disk more exhaustively, more tests need to be run from ¾ T_{scuff} to T_{scuff} to continue the transition to scuffing, e.g. 0.8 T_{scuff}, 0.9 T_{scuff}, and perhaps 0.95 T_{scuff}.

Chapter 2. Conclusions and Recommendations

2.1 Summary from This Study

The study of roughness has come a long way. From the birth of GW statistical contact model in the 1960's, which is now a classic theory to many researchers, to recent Birmingham-14, the method of characterizing surface roughness is every bit rich and diverse. It is known that roughness, or the texture of surface topography, is an integral part of many applications where contact/sliding is involved. Roughness is not just geometry of a surface, but also an important factor that may determine the device performance. The focus of this work is to distinguish noteworthy set of roughness parameters, which can provide a satisfactory geometrical and functional characterization of the surface topography. In Chapter 2, various types of roughness characterization techniques in both 1-D and 2-D are summarized by using different types of surfaces, for example, magnetic storage media surfaces. Although the simple Bush-Gibson-Thomas isotropic model (1-D) and Sayles-Thomas anisotropic model (2-D) owe their success to Nayak's original mastery in spectral moment study, the extent of which their roughness parameters describe the surface topography is still not comprehensive. Therefore, a set of new 2-D parameters, termed "Birmingham-14," has been introduced as something meritable to investigate throughout this roughness research.

The Birmingham-14 not only includes the equal counterparts to the 4 roughness parameters suggested by the spectral moment approach (i.e. σ_s, D_{summit}, R, γ), but it offers 10 more parameters that cover the aspects of amplitude, spatial, hybrid, and functional characteristics of 2-D topography. From the direct comparison between the spectral moment roughness values and the Birmingham-14 values, it has been numerically substantiated that the Birmingham-14 is indeed a reliable and yet versatile set of parameters. It can be used to analyze any surface, from the air conditioning compressor surfaces undergoing wear evolution leading to scuffing (Chapter 5), to the extremely smooth high density recording disk media surfaces (Chapters 2, 3, 4).

2.2 Main Conclusions and Recommendations

Several conclusions can be made based on the extensive surface roughness characterization performed in this work.

1.) The roughness parameters offered by the 2-D spectral moment (i.e. σ_s, D_{summit}, and R), and the Birmingham-14 counterparts (i.e. S_q, S_{ds}, and S_{sc}) do not differ much from one another numerically, except in the case of the parameters describing the measure of isotropy of the surface, (i.e. γ vs. S_{tr}). It is shown that the measure of anisotropy estimated by the Birmingham-14 is frequently hgher than that estimated by the spectral moments (i.e. $S_{tr} < \gamma$), due to the use of the autocorrelation function in the former. From the author's numerical analysis, autocorrelation is found to be easily influenced by filtering specification (e.g. high-pass/low-pass/band-pass, and cutoff wavelengths, etc), which consequently changes the S_{tr} values significantly. The γ values in many cases are not affected by filtering as much as the S_{tr}, values, hence more reliable.

2.) It is in the remaining 10 parameters, especially in the functional parameters, that the Birmingham-14 can be useful in its description of the surface topography. This is especially proven true when

studying the wear evolution in the surface topography. While wear does influence the amplitude parameters, its full effect cannot be understood on the amplitude parameters alone, for wear may not necessarily decrease the amplitude parameters all the time. Functional parameters, on the other hand, are more reliable parameters when understanding the effects of wear and the implied functional significance (i.e. lubrication retention, material/void volume, etc.).

3.) Unlike in the case of the spectral moment roughness analysis, user's prior knowledge on gross texture directionality is not needed in the Birmingham-14 characterization. Using the power spectrum density analysis, the texture direction can be extracted accordingly, without disturbing the rest of the roughness parametrization.

4.) Due to the limitation on measuring instruments, one essentially cannot perform the analysis over an entire surface. Therefore, it becomes critical to obtain several topographical images to allow statistical variation in the following roughness parameters.

5.) Because of the discretization process involved in the data acquisition, the presented topographical data cover broad bandwidth of wavelengths that may or may not have been exhibited on the original surfaces. Filtering must be performed to maintain only the roughness components. Similarly, effects of waviness can be studied after filtering is performed to keep only the waviness components.

6.) The scale-of-measurements, or scale-effects influence the roughness parameters significantly. When doing the statistical roughness analysis, the appropriate scan may differ from application to application. Therefore, one must always perform scale study at least to some level, to justify the validity in the values of the roughness parameters (Chapter 4). The RMS scale study seems to be adequate, based on the data shown in Chapter 3.

7.) In dynamic conditions, low-frequency waviness is often more critical than high-frequency roughness. A prime example is found in head-disk interface (HDI) in which flyability of the slider over the disk media is not determined by the roughness of the media, but by the waviness featured in the media under dynamic conditions. Just as the Birmingham-14 standard is used to characterize the surface *roughness*, it can also be used to characterize the surface *waviness*. Future work on the topographical characterization may involve investigation of the Birmingham-14 on waviness.